11-25-2015

Diffusion Tensor Imaging Based Tractography of Human Brain Fiber Bundles

Fahmida Kishowara Chowdhury

DIFFUSION TENSOR IMAGING BASED TRACTOGRAPHY OF HUMAN BRAIN FIBER BUNDLES

by

Fahmida Kishowara Chowdhury

A Thesis

Submitted in Partial Fulfillment of the

Requirements for the Degree of

Master of Science

Major: Electrical and Computer Engineering

The University of Memphis

December 2015

ACKNOWLEDGEMENTS

First and foremost, I would like to thank Dr. Eddie Jacobs, the supervisor of my master's thesis, for his continuous support, patience, motivation, and guidance. I would also like to thank Dr. Gene Reddick of St. Jude Children's Research Hospital for his funding and consistent supervision. Without his cooperation, it would not have been possible for me to complete the thesis.

I am also grateful to St. Jude Children's Research Hospital for providing me with the MRI/DTI data sets that I used in my research.

A special "thank you" to my husband and lab mate, Jakir Hossen, for his constant support and encouragement throughout the journey. Finally, I would like to thank my parents and all of my family members for their love and unconditional support.

ABSTRACT

Tractography is a non-invasive process for reconstruction, modeling and visualization of neural fibers in the white matter (WM) of human brain. It has emerged as a major breakthrough for neuroscience research due to its usefulness in clinical applications. Two types of tractography approaches: deterministic and probabilistic have been investigated to evaluate their performances on tracking fiber bundles using diffusion tensor imaging (DTI). The images are taken by applying pulsed magnetic fields in multiple gradient directions. After removing the non-brain areas from the images, the diffusion tensor indices for each image voxel are calculated.

White matter connectivity of the brain, i.e. tractography, is primarily based upon streamline algorithms where the local tract direction is defined by the principle direction of the diffusion tensor. Simulations are performed using three approaches: fiber assignment by continuous tracking (FACT), probability index of connectivity (PICo) and Gibbs tracking (GT). Simulation results show that probabilistic tractography i.e. PICo and GT can reconstruct longer length of fibers compared to the deterministic approach-FACT but with a cost of high computation time. Moreover, GT handles the more complex fiber configurations of crossing and kissing fibers, more effectively and provides the best reconstruction of fibers. In addition, diffusion tensor indices: fractional anisotropy (FA) and mean diffusivity (MD) for a region of interest can be quantified and used to assess several brain diseases. Prospective investigation of DTI based tractography can reveal useful information on WM architecture in normal and diseased brain which will speed up the detection and treatment of various brain diseases.

TABLE OF CONTENTS

LIST OF TABLES

LIST OF FIGURES

CHAPTER 1

INTRODUCTION

1.1 Overview

Diffusion tensor imaging (DTI) has emerged as a powerful method for investigating white matter architecture in-vivo and non-invasively. The process of using DTI data to obtain explicit information on white matter structures i.e., how human brain fiber bundles are connected, is commonly known as tractography. Recently, DTI based tractography has been given much attention due to its applications in several medical fields such as patients with acute stroke or brain tumors, neurodegenerative disorders including multiple sclerosis (hardening or thickening of tissue), epilepsy, Alzheimer disease, autism, and movement disorders [3]. DTI enables visualization and characterization of white matter fascicles (i.e. bundles of brain fibers) in two and three dimensions. A sample of superior longitudinal fascicle is shown in Fig. 1.

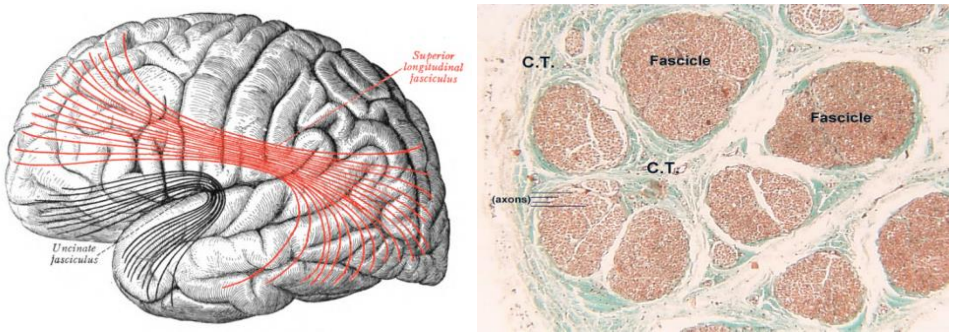

(a) (b)

Fig. 1: (a) superior longitudinal fascicle (b) cross section of brain fascicle [6]

In general, it measures the displacement of water molecules on the micron scale and yields information about white matter (WM) fibers that pass within a voxel. Water molecules contain protons, which become aligned in a magnetic field. Motion or diffusion of water molecules is found to be much faster along the WM fibers than perpendicular to them [2]. The difference between the two motions (parallel and perpendicular to fibers) is the basis of DTI which is also termed diffusion anisotropy. DTI gradient directions are the list of vectors that describe the diffusion weighting directions for DTI acquisition on an MRI scanner. To observe the diffusion in all directions, many diffusion weighted images with diffusion weighting gradients are acquired in different directions. From these diffusion-weighted images, a 3D description of the direction for the diffusion of water within a voxel is inferred. Diffusion in white matter is anisotropic in nature and an ellipsoid is used to represent diffusion directions as shown in Fig. 2. These directions of water diffusion are tracked in DTI based tractography.

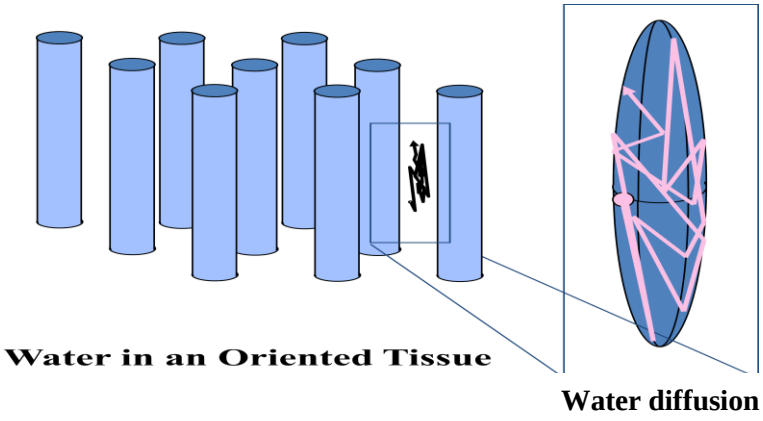

Fig. 2: Anisotropic nature of water diffusion [14]

Two different approaches to tractography are considered in this research: deterministic and probabilistic. In deterministic tractography, the reconstruction of long neuronal pathways occurs in small successive steps by following the local direction of the fiber in a given voxel. This method is computationally efficient, but minor errors in the determination of a local step may significantly affect the final path, making the method unstable. More recently, probabilistic approach based tractography methods have become predominant. It can also be used on a global scale (referred to as global tractography) to create a connectivity map between distinct regions of the brain's gray matter as shown in Fig. 3.

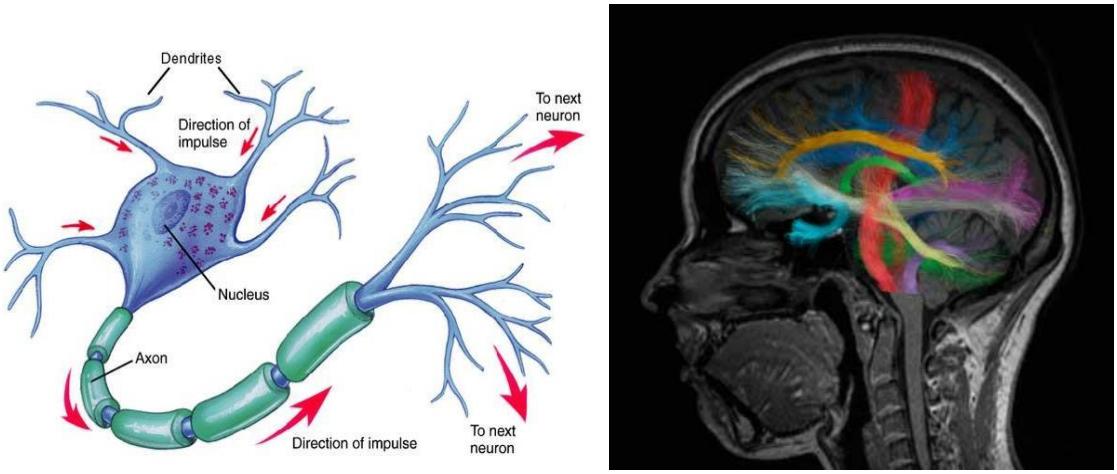

(a) (b)

Fig. 3: Image of (a) single neuron structure and (b) human brain fiber bundles tractography [5]

Global tractography methods [8] try to reconstruct the fiber paths simultaneously while finding the configuration that minimizes the difference between the measured data and the reconstruction. This tracking is more stable in the presence of noise and imaging artifacts in the data.

1.2 Background

Magnetic resonance imaging (MRI) is a medical imaging technique that produces detailed images of organs, tissues, bone and other internal body structures using a powerful magnetic field, radio frequency pulses and a computer. It is a non-invasive way to create image volumes in which slices can be viewed at any location and direction. It is widely used in hospitals for medical diagnosis, staging of disease and for follow-up without exposure to ionizing radiation.

In 1979, the first clinical MRI studies appeared and during that same year the first commercial MRI scanner was manufactured by Fonar based on a heavy permanent magnet. The MRI market increased because of higher field strength air core resistive electromagnets that were lighter in weight but required approximately 40 kW of electrical power [1].

In the late 1980s, Hawksworth et al. proposed an electromagnetic self-shielding concept that eliminated the need for the heavy iron yoke or room shields previously required for siting high-field magnets. The practical and economic operation of superconducting MRI magnets requires the development of cryogenic systems with very low thermal losses. The evolution of such MRI cryostats has been significant over the past 25 years, and they have developed from simple liquid helium, liquid nitrogen shielded reservoirs with relatively high cryogen evaporation rates to single or multi-cryocooled cryostats providing nominally zero-boil-off conditions. Recently, the typical requirements for a whole body imaging magnet include a central field uniformity of a few ppm (mostly in a spherical volume of around 45 cm) and a temporal field stability of better than 0.05 ppm/h. The self-shielding concept is applied routinely for field strengths

up to 4 T for whole body systems and is currently being introduced also for 7 T systems [1]. Magnetic resonance measurements are made of collections of spins. Nuclear spins is an intrinsic property of an atom and its value depends on the precise atomic composition.

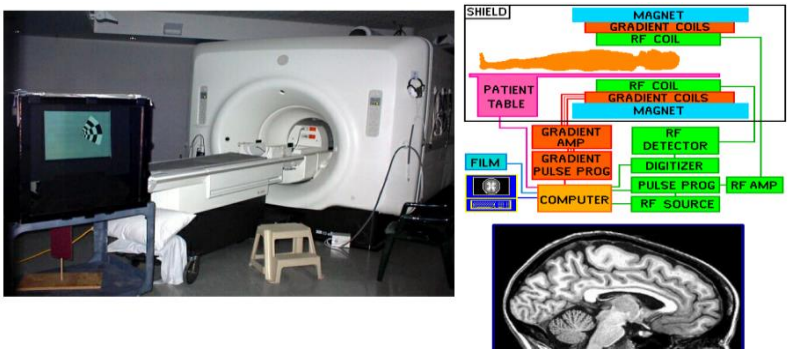

Fig. 4: Schematic diagram of an MRI machine [13]

One can consider that spin is constantly rotating around its own axis causing it to behave like a tiny magnet oriented from the North Pole to the South Pole. This generates a magnetic moment vector that is parallel to the axis of rotation. The directions of magnetic moments are usually considered random because the orientation of the individual particles is unknown, so the total magnetic moment over several particles is zero [2] as shown in Fig. 5 (a).

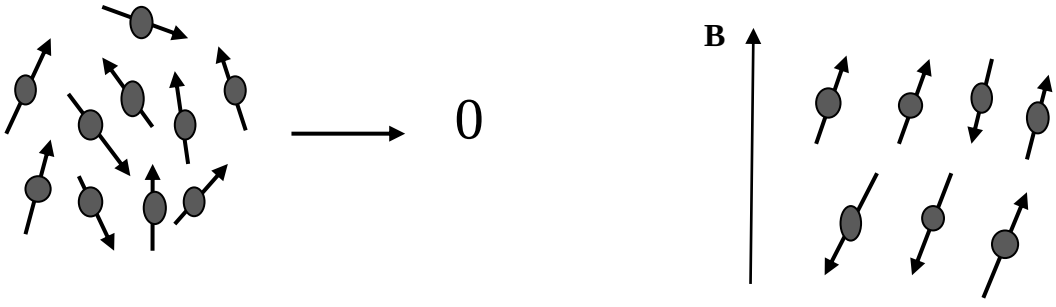

(a) (b)

Fig. 5: (a) without an external magnetic field, the protons have their spin vectors oriented randomly. The vector sum of these spin vectors is zero. (b) By applying external magnetic field, spin vectors are aligned parallel or anti parallel to the field.

When an external magnetic field is applied to a group of particles, there is an interaction or coupling happens between the proton and the magnetic field which is known as Zeeman interaction. This coupling causes a difference in energy between proton aligned parallel and anti parallel to the field as shown in Fig. 5(b). The result is that spins in the two orientations, parallel and anti parallel have different energies. The parallel orientation is of lower energy than the anti parallel orientation. In the magnetic field, the numbers of protons oriented parallel to the field are greater than the anti parallel oriented protons that induce polarization of the spin orientation. The exact number of protons in each energy level is governed by a distribution known as the Boltzmann distribution:

$$\frac{N_{upper}}{N_{lower}} = e^{\frac{-n}{kT}} \tag{1.1}$$

Where N_{upper} represents the number of spins in the higher energy level, N_{lower} indicates the number of spins in the lower energy level, k is Boltzmann's constant and T is the temperature in Kelvin.

Once all the particles are aligned and placed in these two distinct states, it is possible for the particles in the lower state to transition to the higher state by absorbing photons containing the exact amount of energy in the energy gap between the states. The energy difference is proportional to the resonant frequency and thus the magnetic field B_0 :

$$\Delta E = h\omega_0 = h\gamma B_0/2\pi \tag{1.2}$$

where h is the Planck's constant.

Although an individual proton absorbs the radio frequency (RF) energy, it is more useful to discuss the resonance condition by examining the effect of the energy absorption on the net magnetization, M_0. For a large number of protons such as in a volume of tissue, there is a significant amount of both absorption and emission occurring during the RF pulse. However, because there are more protons at the lower energy level, there will be a net absorption of energy by the tissue. The energy is applied as an RF pulse with a central frequency ω_0 and an orientation perpendicular to B_0, as indicated by an effective field B_1 shown in Fig. 6. This orientation difference allows a coupling between the RF pulses and M_0 so that energy can be transferred to the protons.

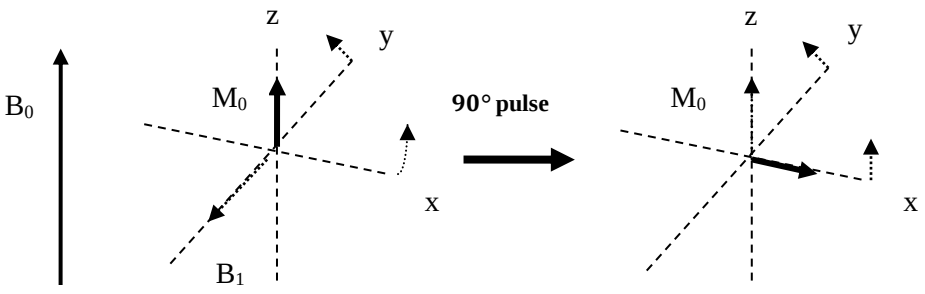

Fig. 6: Absorption of energy by protons from a 90^0 RF pulse and rotation of M_0 into the transverse plane.

Absorption of the RF energy of frequency ω_0 causes M_0 to rotate away from its equilibrium orientation. The direction of rotation of M_0 is perpendicular to both B_0 and B_1. If the transmitter is left on long enough and at a high enough amplitude, the absorbed energy causes M_0 to rotate entirely into the transverse plane, a result known as a 90° pulse. When viewed in the rotating frame, the motion of M_0 is a simple vector rotation; however, the end result is the same whether a rotating or stationary frame of reference is used. When the transmitter is turned off, the protons immediately begin to realign

themselves and return to their original equilibrium orientation. They emit energy at frequency ω_0 as they do so.

Relaxation is a fundamental process in MR by which protons release the energy that they absorbed from the RF pulse. In resonance absorption, RF energy is absorbed by the protons only when it is transmitted at the correct frequency. Although an individual proton absorbs the energy, relaxation times are measured for an entire sample and are statistical or average measurements. Two relaxation times can be measured, known as T1 and T2. Both times measure the spontaneous energy transfer by an excited proton, but they differ in the final disposition of the energy. The relaxation time T1 is the time required for the z component of M to return to 63% of its original value following an excitation pulse. T1 relaxation provides the mechanism by which the protons give up their energy to return to their original orientation. The relaxation time T2 is the time required for the transverse component of M to decay to 37% of its initial value via irreversible processes.

In clinical MRI, the RF-pulse is selected with the frequency corresponding to the energy difference required for protons in water molecules to transition between energy states. The released energy is related to the number of hydrogen nuclei. The T1 relaxation gives information on the chemical surrounding of the water and the T2 relaxation reflects the surroundings of each individual atom, which gives a different contrast. The tissues are separated with the help of these variables as they show different characteristics in T1 and T2 relaxation time.

The development of magnetic resonance imaging (MRI) has led to the design of numerous imaging techniques. Among them, diffusion tensor imaging (DTI) assesses white matter changes in the patients that are not normally seen on conventional MRI. The relationship between the signal intensity of the diffusion weighted images S, diffusion sensitizing field gradient based on Stejeskal Tanner spin echo scheme and the signal value S_0 without the gradient is given in (1.3):

$$\mathrm{S} = \mathrm{S}_0 \mathrm{e}^{-\gamma^2 \mathrm{G}^2 \delta^2 (\Delta - \frac{\delta}{3}) \mathrm{D}_{\mathrm{app}}} \tag{1.3}$$

where γ is the gyromagnetic ratio of proton, δ and G represent the duration and the magnitude of the motion probing (or diffusion sensitizing field) gradient, Δ is the time between the centers of the pair of gradient pulses, and D_{app} is a scalar value called the apparent diffusion coefficient (ADC) which reflects molecular diffusivity under motion restriction such as fluid viscosity.

In DTI, the diffusion coefficient is a 3 ×3 symmetric positive semi-definite matrix as shown in (1.4).

$$D = \begin{pmatrix} D_{xx} & D_{xy} & D_{xz} \\ D_{xy} & D_{yy} & D_{yz} \\ D_{xz} & D_{yz} & D_{zz} \end{pmatrix} \rightarrow \begin{pmatrix} \lambda_1 & 0 & 0 \\ 0 & \lambda_2 & 0 \\ 0 & 0 & \lambda_3 \end{pmatrix} \text{ and } (\vec{\varepsilon}_1, \vec{\varepsilon}_2, \vec{\varepsilon}_3) \tag{1.4}$$

Where λ_1, λ_2 and λ_3 are eigenvalues representing diffusivity along the axes whose directions are retained in unit eigenvectors $(\vec{\varepsilon}_1, \vec{\varepsilon}_2, \vec{\varepsilon}_3)$.

The largest eigenvector of the diffusion tensor as shown in Fig. 7 is assumed to be oriented parallel to the local fiber tracts, which can be reconstructed in a brain dataset by following paths in the estimated eigenvector field.

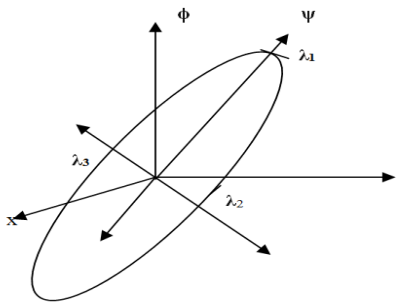

Fig. 7: Diffusion tensor represented by an ellipsoid ($\lambda_1 \geq \lambda_2 \geq \lambda_3$)

One of the most important factors in DTI acquisition is gradient direction. At least 6 gradient directions are required to calculate the diffusion tensor [4]. If gradient directions are increased, more diffusion weighted images are used to calculate the diffusion tensor, resulting in more accurate tensor estimation but much longer imaging time [7].

A long thin ellipsoid means very good diffusion for water along the long axis of that ellipsoid. The mean diffusivity (MD) and fractional anisotropy (FA) as shown in (1.5) and (1.6) respectively are the most widely used indices for representing the motional anisotropy of water molecules. These measures are sensitive to the presence and integrity of WM fibers [11, 12]. Color coded FA maps are the way to show the directional information embedded in DTI.

$$MD = \frac{\lambda_1+\lambda_2+\lambda_3}{3} \tag{1.5}$$

$$FA = \sqrt{\frac{3}{2}} \times \sqrt{\frac{(\lambda_1-MD)^2+(\lambda_2-MD)^2+(\lambda_3-MD)^2}{\lambda_1^2+\lambda_2^2+\lambda_3^2}} \tag{1.6}$$

These indices help to detect brain diseases. For example, in case of pediatric multiple sclerosis, the value MD increases and FA decreases compare to their normal value [9, 10]. After collecting the information of diffusion tensor, tractography is done using deterministic or probabilistic methods. Deterministic tractography methods are primarily based upon streamline algorithms where the local tract direction is defined by the major eigenvector of the diffusion tensor [1]. Tracking the crossing and kissing white matter tracts is a challenge for deterministic process. This limitation can be solved using global tractography which will be discussed later.

1.3 Objectives

The objective of this thesis is to

- Calculate region of interest (ROI) basis diffusion tensor indices (fractional anisotropy, mean diffusivity, relative anisotropy etc.) from DTI datasets.
- Simulate a DTI dataset considering multiple gradient directions (12D, 20D, 30D, 64D) using deterministic approach (Fiber Assignment of Continuous Tracking).
- Simulate a DTI dataset considering multiple gradient directions (12D, 20D, 30D, 64D) using probabilistic approach (PICo).
- Simulate a DTI dataset considering multiple gradient directions (12D, 20D, 30D, 64D) using global tractography approach (Gibbs Tracking).
- Compare and contrast performance of deterministic and probabilistic tractography approaches.
- Simulate three datasets (All 64D) taken before and after radiation therapy to show the effect.

CHAPTER 2

STATE OF THE ART

2.1 Diffusion Tensor Imaging (DTI):

Diffusion tensor imaging (DTI) also known as diffusion magnetic resonance imaging (DMRI) is a magnetic resonance imaging technique first introduced in the mid 1980s [18] and during the past 35 years has played an important role in MRI of the central nervous system. Diffusion MRI measures the diffusion of water molecules in biological tissues. In other words, water molecules are used as a probe that can reveal microscopic details about tissue architecture, either in a normal or diseased state. The human body is composed of tissues that contain primarily water and fat, both of which contain hydrogen. Clinically, DTI is useful for the diagnoses of conditions (e.g., stroke) or neurological disorders (e.g., multiple sclerosis), and helps better understand the connectivity of white matter axons in the central nervous system. According to turbulence and Brownian motion, the movements of water molecules are random in an isotropic medium. However, the diffusion may be anisotropic in biological tissues where the Reynolds number is low enough for flows to be laminar. For example, a molecule inside the axon of a neuron has a low probability of crossing the myelin membrane. Therefore, the molecule moves principally along the axis of the neural fiber. It is assumed that the majority of the fibers are parallel to the principle direction if the molecules in a particular voxel diffuse in that direction.

Another application of diffusion MRI is diffusion-weighted imaging (DWI). Following an ischemic stroke, DWI is highly sensitive to the changes occurring in the lesion. It is surmised that in case of cytotoxic edema (cellular swelling), the signal on

DWI scan increased due to the increment of restriction (barriers) to water diffusion. The DWI enhancement appears within 5–10 minutes of the onset of stroke symptoms (as compared to computed tomography, which often does not detect changes of acute infarct for up to 4–6 hours) and remains for up to two weeks. Coupled with imaging of cerebral perfusion, researchers can highlight regions of "perfusion/diffusion mismatch" that may indicate regions capable of salvage by reperfusion therapy.

Diffusion-weighted images are MR images with signal intensities sensitized to the random motion of water molecules. A water molecule, or spin, that migrates along trajectory path, $r(t)$, through a gradient field given by the waveform, $G(t)$, accumulates phase, φ, according to (2.1)

$$\varphi(t) = -\gamma \int_0^t \overrightarrow{G(t')} \cdot \overrightarrow{r(t')}\, dt' \tag{2.1}$$

where γ is the gyromagnetic ratio. For the condition where there is a large number of spins (e.g. water molecules in a voxel) having random trajectories, the net phase shift averaged over all spins is close to zero because of almost equal numbers of positive and negative phase shifts. So unlike coherent directional motion through a gradient field that results in measurable phase such as in flow MR imaging, a large number of randomly migrating spins yields no net phase shift, rather spin dephasing manifests as signal attenuation. Moreover, the degree of signal attenuation increases as the breadth of the distribution of phase shifts increases. Equation 2.1 indicates phase shift (thus phase distribution width) increases with a longer integral interval, greater gradient strength, gradient duration, and/or greater migration path or mobility.

Due to random spin diffusion, the signal attenuation is presented by equation 2.2

$$S(t) = S_0 e^{-D\int_0^t \overrightarrow{k(t')}\cdot\overrightarrow{k(t')}dt'} \tag{2.2}$$

where *S(t)* is the diffusion attenuated signal, S_0, is the signal without diffusion attenuation, *D* is the spin diffusion coefficient, and *k(t)* relates to the time integral of the gradient waveform given by-

$$\overrightarrow{k(t)} = \gamma \int_0^t \overrightarrow{G(t')}\, dt' \tag{2.3}$$

Equations 2.2 and 2.3 are written in general form for arbitrary gradient waveforms. Usually diffusion sensitization gradients are incorporated within an imaging sequence, in which case, the imaging and diffusion components of the gradient waveform should be included in the equations. Ignoring imaging for a moment, the simple two-pulse gradient waveform shown in Fig. 8, often referred to as the Stejskal-Tanner pulsed field gradient (PFG) (Stejskal et al. 1965), is the default diffusion sensitive sequence.

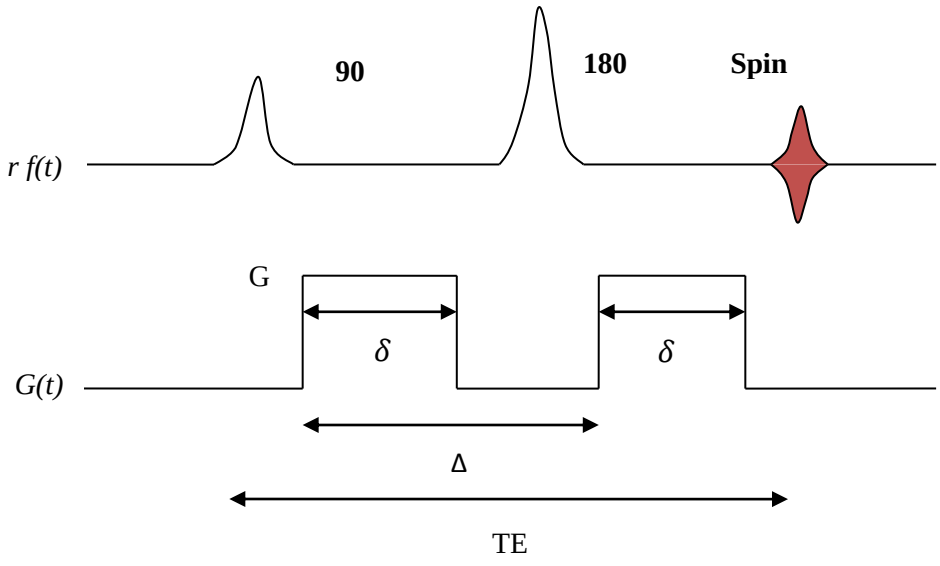

Fig. 8: Standard pulsed field gradient (PFG) waveform for diffusion sensitization

Now the b value can be written as-

$$b = \int_0^{TE} \overrightarrow{k(t')} \cdot \overrightarrow{k(t')}\, dt' = (\gamma G \delta)^2 \left[\Delta - \frac{\delta}{3}\right] \tag{2.4}$$

Frequently, only the gradient amplitude is altered to vary *b*-value in a diffusion imaging sequence. This leads to change in signal as a function of *b*-value, from which the diffusion coefficient is calculable from a minimum of two *b*-value settings:

$$S(b) = S_0 e^{-Db} \tag{2.5}$$

$$\text{or} \qquad D = \frac{1}{(b_2 - b_1)} \ln \left[\frac{S(b_1)}{S(b_2)}\right] \tag{2.6}$$

Often one of the PFG gradients has zero amplitude, in which case $b_1 = 0$ and $S(b_1) = S_0$ The formalism above only considers isotropic molecular diffusion. But neuro tissue can be highly anisotropic where the apparent water mobility varies several-fold based on relative orientation of measurement axis and myelinated white matter fiber tracts. For the anisotropic system, the single valued diffusion coefficient from equation 2.4 is generalized to a 3 × 3 second order rank diffusion tensor. Moreover, generalizations of (2.4) and (2.6) are as follows-

$$b_{ij} = \gamma^2 \int_0^{TE} \left(\int_0^{t'} G_i(t")dt"\right) \cdot \left(\int_0^{t'} G_j(t")dt"\right) dt' \tag{2.7}$$

$$\text{and} \qquad \ln\left(\frac{S_0}{S_b}\right) = \sum_{i=1}^{3} \sum_{j=1}^{3} b_{ij} D_{ij} \tag{2.8}$$

Where $b = 0$ is an isotropic measurement of S_0 and i and j indices relate to any three gradient directions [x, y, z]. The b_{ij} elements are the anisotropic corollary to the isotropic b-factor and are calculated for each gradient condition of a directionally sensitive

diffusion acquisition [17]. At least six non-collinear diffusion gradient directions (plus $b = 0$) are required to determine the diffusion tensor. Once the diffusion tensor is determined, it is very important to summarize the information in an understandable way since there are now six unique diffusion values for each pixel in the image. This type of imaging technique is known as diffusion tensor imaging (DTI).

The recent development of DTI enables diffusion to be measured in multiple directions and the diffusion indices for each voxel is calculated in each direction. This technique allows researchers to make brain maps of fiber directions to examine the connectivity of different regions in the brain (using tractography) as well as examine areas of neural degeneration and demyelination in case of brain diseases.

2.2 Tractography

Diffusion weighted magnetic resonance imaging is a technique to study the anatomical and functional brain relationships as well as for the discovery of functional distinctions between cortical regions of the brain [24]. It's a non-invasive tool for characterizing WM injury and neuro-degenerative diseases before surgery and for many other clinical applications. The tracking of human brain fiber bundles are based on the principle direction of diffusion of tensor in each voxel. An important limitation of the DT model arises from the Gaussian diffusion assumption which states that there can only be a single fiber population per voxel. Water diffusion in biological tissues, especially the brain, is not free and cannot be modeled by a single Gaussian distribution. A recent study estimates that one-third of white matter voxels contain more than one fiber bundle orientation [20]. Moreover, the ADC depends on various experimental and technical parameters such as the actual diffusion coefficient of water molecule populations

presenting in an MRI voxel, the voxel size, the diffusion time or the degree of sensitization of MR images to diffusion (i.e. b- value). Thus, it is possible to follow false tracts during tractography using DT. To overcome these limitations of the DT, new High Angular Resolution Diffusion Imaging (HARDI) techniques have been developed. Most of these methods produce representations of water molecule diffusion as a function of direction such as in the cases of Diffusion Spectrum Imaging (DSI), Q-Ball Imaging (QBI), Composite Hindered and Restricted Model of Diffusion (CHARMED), Persistent Angular Structure (PAS), Diffusion Orientation Transform (DOT) and multi tensor distributions. Application of each of these methods results in various representations of the angular diffusion profile. For example, the principal directions extracted from the Orientation Distribution Function (ODF) [21] can be interpreted as principal directions of the underlying fiber architecture. Otherwise, spherical deconvolution (SD) or mixture models [22] are used to estimate the distribution of the fiber directions within a voxel (fiber ODFs). There are two essential procedures to create a reliable map of brain connectivity using so called fiber tractography: the first step is to accurately estimate fiber orientations using an adequate diffusion reconstruction method and the second step is to implement a robust fiber tracking algorithm [18]. Tractography algorithm techniques are categorized by two methods:

1. Deterministic tractography and
2. Probabilistic tractography.

There are various deterministic tractography techniques such as connect the voxels [conturo] and Fiber Assignment by Continuous Tracking (FACT) [Mori]. FACT is a

widely used streamline-based deterministic method that traces pathways from a seed region by following the primary eigenvector from one voxel to the next [23].

2.2.1 Deterministic tractography:

Deterministic tractography methods are primarily based upon streamline algorithms where the local tract direction is defined by the major eigenvector of the diffusion tensor. These approaches provide information about the white matter anatomical connection and organization in different regions of the brain. The accuracy and variance of the reconstruction process depends on the tractography algorithm, the signal-to-noise ratio, the diffusion tensor eigenvalues, and the tract length. However, crossing and branching white matter tracts create significant challenges for the reconstruction. Some deterministic tractography methods are discussed below.

Connect the voxel:

In this approach, the local tensor orientation from each voxel is obtained from DTI. The fiber directions are connected to reconstruct the entire pathways by propagating through each voxel from a designated starting point (seed point) and following the fastest diffusion direction until it reaches a termination point. Tracks are terminated where diffusion anisotropy fell below an assigned threshold, typically in gray matter.

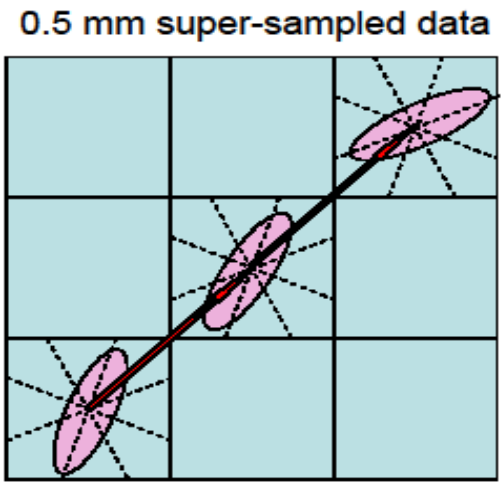

Fig. 9: Connect the voxel tractography [25]

To define the direction of the next voxel, the tensor D and its eigenvector corresponding to the largest eigenvalues are calculated at each voxel, from interpolated DT-MRI data. By repeating this procedure multiple times for every seed point above the threshold, tracking of whole brain is achieved [25].

FACT:

The fiber assignment by continuous tracking (FACT) algorithm is a streamline tracking algorithm, which takes the principal direction of voxel to track the fiber direction. The algorithm uses the whole diffusion tensor matrix to determine the tracking direction. In clinical applications, it is the most commonly used method. However, the main limitation of this algorithm is that it cannot resolve the fiber crossing issue, which results in much shorter or sparser fibers. Several novel methods like Gibbs tracking has recently been proposed to overcome the crossing and kissing fiber issue.

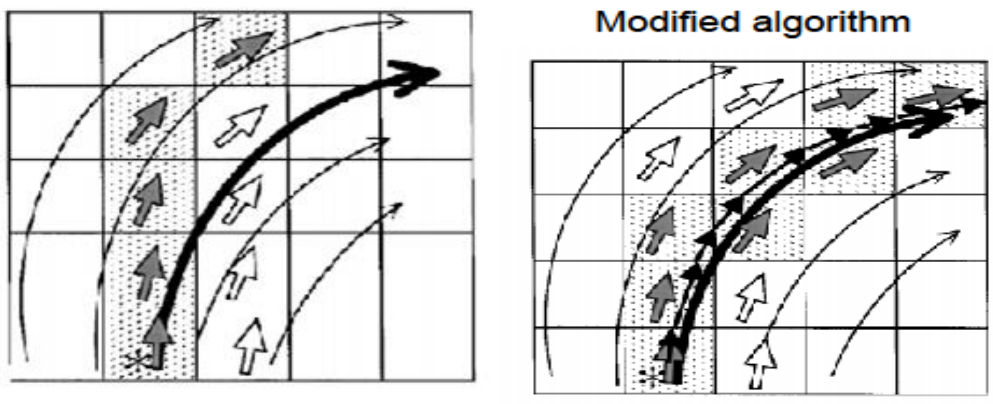

Fig. 10: Fiber assignment by continuous tracking [31]

In each voxel, the FACT algorithm takes the corresponding eigenvector of the biggest eigenvalue as the fiber tracking direction [31]. This is complimented in a continuous coordinate space. Considering a start point's coordinate x_t, which has corresponding eigenvector $\overrightarrow{e_{1t}}$ and the step Δ_t, the next point's coordinate x_{t+1}can be expressed as,

$$x_{t+1} = x_t + \overrightarrow{e_{1t}} \times \Delta t \ . \tag{2.9}$$

All the points tracked into a line are then connected, forming a fiber according to the start point. For a given region of interest (ROI), all the fibers are tracked accordingly. But the tracking process should meet some criteria.

First, the threshold value for fractional anisotropy (FA) is set to 0.2, which is considered as the boundary value between white matter and gray matter; because the FA values of gray matter are usually lower than 0.2. Another threshold value for FACT is the curvature between two consecutive steps which is set to 90°. The liberal curvature is chosen to allow the detection of strong fiber bending. Second, the deflection angle

threshold setting is typically set to 45°-70° because the probability of sharp turns between two adjacent neurons is close to zero in the white matter of the human brain.

This method, and the computation involved is simple and easy to understand. This computation can effectively perform fiber visualization in a region with significant diffusion anisotropy. Nevertheless, when a region with fiber crossing is encountered, the tracking is partially finished or interrupted, resulting in shorter or sparser fibers. This approach leads to erroneous results if there are fibers within a voxel running in different directions. In addition, fibers with a strong curvature may be difficult to reconstruct.

2.2.2 Probabilistic Tractography:

The probabilistic algorithm assumes a distribution of orientations and defines pathways by generating multiple curves from seed points using several methods like probability index of connectivity (PICo) [19] and Bayesian method [30]. The probability of connectivity is then assigned to individual voxels based on the frequency with which the curves traverse the voxels. Probabilistic tractography assesses the probability that a voxel is connected to a given start point, by means of iterative random walks. This method exploits the statistical nature of the information obtained by DWI and determines the most probable fiber pathway.

PICo:

A number of methods have been used to generate distributed maps of the degree or probability of connectivity in different brain regions. In particular, to assess the cerebral connectivity, the diffusion process is simulated with the aim of establishing connectivity in a probabilistic way using a Monte Carlo processes. For example, a grid-based random walk process may be simulated, in which a particle is allowed to diffuse at

a rate determined by a function of the magnitude of the diffusion coefficient along one of the possible inter-grid point (inter-voxel) directions chosen at random. This process continues until the random walk has reached some threshold in allowed tensor anisotropy. After repeating the process a large number of times, an index of the connectivity is provided to each voxel [19]. For the probabilistic connectivity analyses, the uncertainty of the principle eigenvector orientation is exploited for each image voxel. Streamline propagation is repeated using the probability distribution functions (PDFs) describing the inferred distribution in the fiber orientation to establish the confidence of connection to the start point of a distributed area.

Bayesian method:

The probability of a fiber connecting two areas in the brain can be estimated where the probability density function of the local fiber orientation is derived in a Bayesian framework. A white matter fiber can be modeled as a finite-length path:

$$v_{1:n} = v_1, v_2, \dots \dots v_n \tag{2.10}$$

If Ω_A^n is the set of all possible paths of length n that originate from A and probability to each path in the space is $p(v_{1:n})$, we can write

$$\sum_{n=1}^{\infty} \int p(n)p(v_{1:n}) = 1 \tag{2.11}$$

Now, let Ω_{AB}^nbe the set of all possible paths of length n between A and another area B. We can find the probability $p(A \to B|D)$of a fiber going from A to B, given the diffusion data D, by summing the probabilities for all paths of all lengths between these areas

$$p(A \to B|D) = \sum_{n=1}^{\infty} \int p(n)p(v_{1:n}\, D) \tag{2.12}$$

This integral is estimated by applying Monte Carlo methods.

To estimate the maximal probability path, we a need a method for drawing random paths $v_{1:n} = \{v_1, v_2, \dots \dots v_n\}$ from a high dimensional probability density function (pfd) $p(v_{1:n})$. Assume that the step length is fixed. For simplicity and notational convenience, we assume that the vector v_i only depends only on the previous vector v_{i-1}. The probability for a path of a given length n then factors into

$$p(v_{1:n}|D) = p_1(v_1 D) \prod_{i=2}^{n} p_i(v_i v_{i-1}, D) \tag{2.13}$$

The probability function of the step direction is different for every vector in the path as indicated by the indexes of the probability functions. Using this equation, random paths can be built for v_1. Then sequentially, the random direction v_2 can be drawn using v_1 and so on [30]. This process is known as sequential importance sampling. In white matter tractography, this process is named streamlining. The sequential sampling is terminated when the path reaches a certain threshold value or meets a stopping criterion.

Path integral method:

The advantages of this approach over the streamline method are a specific mechanical representation of the tracts, a probabilistic interpretation of the tract solution, and the inclusion of excluded volume interactions.

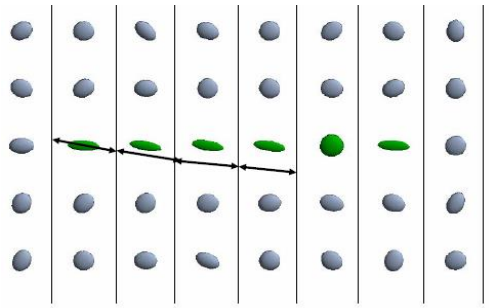

Fig. 11: path integral method [26]

To describe the trajectory of the tract $x(s)$ as a function of the curvilinear coordinate s along the tract, the Lagrangian is written as

$\mathcal{L} = T - V$ where $T = \frac{1}{2a} X^2$ is the Wiener measure, a is the step and $V = V_\varphi + V_K + V_\omega$ is the potential energy of the tract which is comprised of the empirical potential V_φ derived from the diffusion data, the elastic potential energy V_K, and the excluded volume potential $V_\omega$which arises from interaction between tracts. These parameters are used by following the paper [26].

The empirical potential is related to the fiber orientation distribution function which gives the probability distribution for finding a fiber within a differential solid angle around n where n=x/|x| is the bulk direction of the fiber. For the elastic potential of the tract, the Frank free energy [26] is,

$$\mathcal{H}_K = K_1(\nabla \cdot n)^2 + K_2(n \cdot \nabla \times n)^2 + K_3(n \times \nabla \times n)^2 \tag{2.14}$$

where the individual terms of equation 20 represent the bending of tracts, shearing of planes of fibers, and divergence of tracts.

The excluded volume interaction can be included by introducing [26]

$$V_\omega = \frac{\omega}{2} \int dt\, \delta(x(s) - x(t)) \tag{2.15}$$

where ω is the strength of the excluded volume interaction. The partition function for the fiber can then be expressed in terms of the path integral [26]

$$Z(x, L) = \int Dx(s) \exp\{-\beta \int_0^L ds \mathcal{H}\} \tag{2.16}$$

Where $Dx(s)$ represents the integral over all possible fiber paths, $\boldsymbol{\mathcal{H}}$ is the Hamiltonian and $= \frac{1}{kT}$; kT is the thermal energy [26].

2.2.3 Local and Global Tractography:

Tractography techniques can also be divided into two subgroups:

1. Local tractography and

2. Global tractography.

Local Tractography:

Local methods reconstruct fibers one by one independently, without taking into consideration the influence of neighboring fibers. Because of this, local tractography is mostly used to study the white matter in specific predetermined regions where specific tracts are of interest, which is useful for numerous medical applications explained in the introduction. The reconstruction of long neuronal pathways is performed in small successive steps, either deterministically or probabilistically by following the local, voxelwise defined distribution of fiber directions. There are several different approaches for local tractography which fall into two subcategories:

i. Line propagation method and

ii. Energy minimization method.

Line propagation method:

This method uses the local tensor information from each voxel obtained from DTI. To reconstruct the fiber pathways, the propagation through each voxel from a designated starting point is measured with the assumption that the fiber pathway follows the maximum diffusion direction provided by the diffusion tensor. Tractography algorithms use this information to track the whole white matter pathway by inferring the

continuity of fiber paths from voxel to voxel [27]. The pathway reconstruction process continues until it meets the stopping criteria: angular threshold and anisotropy threshold. If the angle between two diffusion directions in adjacent voxels is larger than a certain threshold, the propagation is terminated. This is used to prevent implausible pathways such as a fiber that turns too sharply. Another criterion that stops the propagation when it reaches a voxel with very low to no anisotropy is known as anisotropy threshold. Anisotropy values are low in gray matter and in the areas of the white matter with many crossing fibers where the dominant diffusion direction cannot be distinguished. For the linear line propagation model, large errors occur if the angle transition is large. Even for the interpolation approach, it should be noted that the diffusion tensor calculation assumes that there is no consistent curvature of axonal tracts within a voxel. The presence of curvature violates the assumption that the diffusion process along any arbitrary axis is Gaussian, thereby invalidating the routine tensor calculation. Therefore, it is preferable to set a threshold that prohibits a sharp turn during line propagation. The Streamline algorithm is the most used method for line propagation reconstructions.

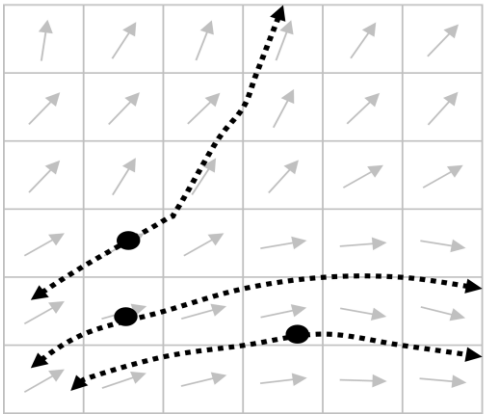

Fig. 12: Line propagation method [27]

This method is fast and suitable to use when one is only interested in the dominant pathway between two predetermined regions of interest.

Energy minimization method:

This technique focuses on finding the most energetically favorable path between two predetermined voxels. The fast marching technique calculates the speed for the spreading front propagation in a certain point using the equation $F(\boldsymbol{r}) = A|\epsilon_1(\boldsymbol{r}) \cdot n(\boldsymbol{r})|$ where A is the anisotropy, ϵ_1 is the eigenvector and n are the orientation normal to the front. This equation indicates that the spreading speed is the largest when the propagating front line is parallel to the eigenvector and minimal when it is perpendicular. Using the equation, the diffusion shape at different time points are represented by multiple contours. A likelihood of connections map is found from these contours. The most likely path is created from the gradient of the steepest path.

Advantages with local methods are mostly that they are fast, but they unfortunately struggle in correctly reconstructing fibers in complicated scenarios such as branching of fibers, fiber kissing, and fiber crossings showed in Fig. 14 due to the limited information given by the diffusion tensor in these scenarios. Local techniques also struggle in reconstructing long fibers due to error accumulation along the propagation route resulting from local noise in each voxel. Local reconstruction methods are therefore unsuitable in their current state for global tractography. This limitation is overcome by other tractography methods, namely global methods.

Global tractography:

Global methods process the entire diffusion information simultaneously and generate a whole-brain reconstruction. This method promises better stability with respect

to noise and imaging artifacts. Because it has a better ability to resolve local fiber orientations, as it considers more than just the local information. Among various global tractography methods, Gibbs tracking and the spin glass method are prominent.

Gibbs tracking:

Gibbs tracking is a powerful global tractography method. This method includes three main steps [28]: (1) Creation of a trial fiber configuration, (2) Calculation of the corresponding DW signal (simulated signal), and (3) Adjustment of the trial configuration with the experimentally measured signal to minimize the difference.

The building elements of reconstructed fibers are small straight cylinders whose length, position and orientation can vary continuously. These cylinders are re-oriented through a process similar the distribution of states in the cooling of an ideal gas. The reconstruction begins at very high "temperature" where the cylinders are randomly distributed in the space occupied by the white matter as shown in Fig 13. The interaction between them results in building long fiber chains with decreasing temperatures. Here, temperature is a time varying parameter as used in simulating annealing methods [32] to find the global optimum solution. The neuronal fibers start and end on predefined surfaces, for example at the boundary with the grey matter. Each cylinder contributes a signal typical for parallel fibers to all voxels it crosses [28].

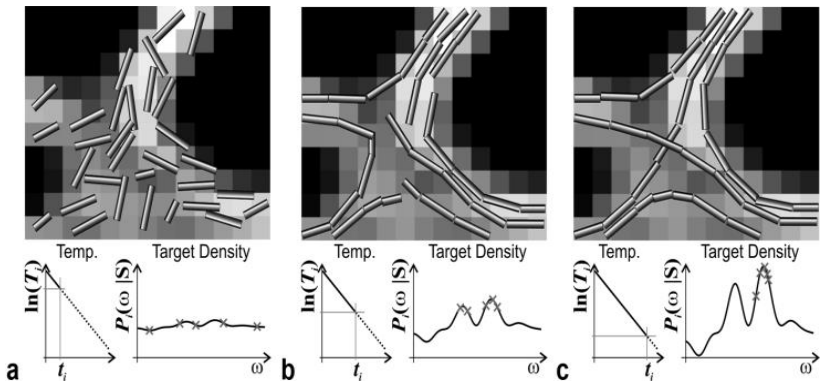

Fig. 13 Principle of Gibbs tracking method; (a) at high temperature (b) at lower temperature (c) temperatures close to zero. [28]

The sum of such contributions is the anisotropic part of the signal. This described method is known as the Gibbs Tracking [28], keeping in mind its close analogy to statistical physics. On the other hand, the described simulation can be considered as a Bayesian approach based on a spatial point processes. The interactions between the cylinders represent the a priori probability and the likelihood function represents the similarity of the measured signal and simulated signal.

Spin glass method:

Spin glass tractography (SGT) is an energy-based paradigm for global tractography. Fiber fascicles are parameterized by small segments called spins which are optimized to minimize a twofold global energy: the first models fidelity to the diffusion data and the second models a low curvature prior [29].

Spins are provided with three types of energies: diffusion potentials, interaction potentials, and generative potentials. Diffusion potentials act as a local non-stationary magnetic field attracting the spin orientations; interaction potentials control the association of spins with neighbors; and the generative potential prevents a spin chain to

end inside the domain by allowing the creation of new spins. A global minimization procedure is used to retrieve the optimal spin configuration.

Global tractography is becoming an emerging approach to studying the structural connectivity of the brain between different regions. It is not currently clinically feasible because of its high computational time. The issue of validation is also important because currently there is no absolute ground truth on the connections existing in real brain tissues.

2.3 Tractography Limitations:

Tractography is a useful tool for tracking human brain fiber connectivity and to detect several brain diseases. But it has some limitations. It cannot follow single neuronal terminations but the principle axis of the diffusion tensor. Another problem is that diffusion tensor tractography assumes a single fiber orientation in each voxel. For voxels where fiber kissing, crossing, or branching happen as shown in Fig. 15, the data extracted from tractography may give an incorrect approximation and is still the focus of current to research. Since ground truth data of brain fiber bundle connections is not available, it is not possible to match the tractography result. Thus, in order to interpret tractography data, some experience and a priori knowledge are required.

(a) (b) (c)

Fig. 14: Fiber (a) crossing (b) branching (c) kissing

2.4 Application DTI tractography

The main application of DTI based tractography is to visualize the neural path of human brain fiber bundles. It has been used to detect several diseases. Some clinical applications are given below:

- It can be used in patients with stroke to visualize damage. The increment of diffusivity at the site of an infarct can be detected by tractography.
- It helps to assess the pathological process in the white matter pathways and introduces the reasons of hardening or thickening of tissue.
- Change in white matter microstructure during neurodevelopment and in aging.
- To identify initial sites for electrocortical stimulation that enables the surgeon to localize the eloquent cortex quicker. It can also help in neurosurgical planning and neuronavigation.
- To measure the loss of neurons in the case of neurodegenerative diseases like Alzheimer disease and epilepsy.
- To identify movement disorders or development disorders like autism, dyslexia etc.

CHAPTER 3

METHODOLOGY

3.1 Tractography Steps

Diffusion tensor imaging studies are gaining popularity among clinicians and researchers due to its increasing applications for studying white matter architecture in vivo, both under healthy and disease conditions. To study the brain network connectivity using DTI, several technical and methodological aspects are taken into account.

The steps of DTI processing for tractography [36] are –

(i) Data acquisition

(ii) Artifacts handling

(iii) Data quality control

(iv) Reconstruction process

(v) Visualization approaches

(vi) Quantitative analysis.

Some of these steps can be done using existing software tools. For the most important step, reconstruction, many researchers are trying to develop their individual techniques with the goal of overcoming the limitations and improving the performance of the tractography. To do so, research is going on to find out the pros and cons of different existing tools and to develop new software tools for each stage of the tractography process. In the following sections, DTI tractography steps are discussed briefly.

Data acquisition:

Diffusion-weighted imaging (DWI) is a simple technique of diffusion imaging that collects images of entire brain through axial slices with no gap between them as shown in Fig. 15. The acquisition is repeated several times while varying the orientation or magnitude of the diffusion gradients. It has low signal to noise ratio (SNR) and resolution and is very sensitive to motion. This sensitivity increases with the intensity and duration of gradient pulses, which are characterized by the *b*-value, the scalar that defines the amount of diffusion weighting in the experiment. In order to get accurate results, the successive images should be in correct order which is ensured by image registration. At least six non-collinear diffusion encoding directions along with a minimally T2 weighted low *b*-image (b = 0 s/mm^2) are required for diffusion tensor estimation. The *b*-value is taken from the range 700-3000 s/mm^2. The spatial resolution is also important for DTI quality and when using isotropic voxels, typically 1.4–2.5 mm^3 is recommended for fiber tracking using interleaved acquisitions to minimize crosstalk between contiguous sections.

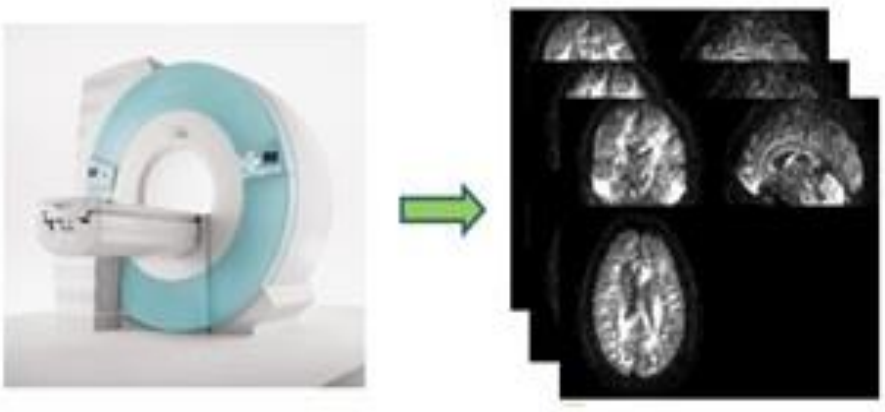

Fig. 15: Diffusion tensor image/data acquisition

Other characteristic parameters of DTI acquisitions are field of view (FOV) usually ranging from 240 to 256 mm, acquisition matrix 96 × 96 –128 × 128, Echo time (TE) 50 –70 ms and repetition time (TR) 8.5 –12s [36].

Artifacts handling:

The main reasons for the presence of artifacts in DWI data sets are the gradient system hardware, pulse sequence, acquisition strategy used, and the head motion. Artifacts in the data sets result in erroneous fiber reconstruction due to incorrect tensor estimation and diffusion maps (FA and MD). Reducing the scan time can minimize the influence of motion artifacts. Several imaging techniques like Single- shot Echo Planar Imaging (EPI), Fast Spin Echo (FSE), Line Scan Diffusion Imaging (LSDI) and Stimulated Echo Acquisition Mode (STEAM) can be used to reduce artifacts [36]. The most prominent artifacts are due to eddy currents (EC) that create geometric distortion in the DW images. Stronger and longer diffusion gradients create ECs in the conductive parts of the magnet. Image registration is done to correct eddy current distortions. Figure 16 illustrates two diffusion tensor images before (left) and after (right) applying the eddy current correction technique [37].

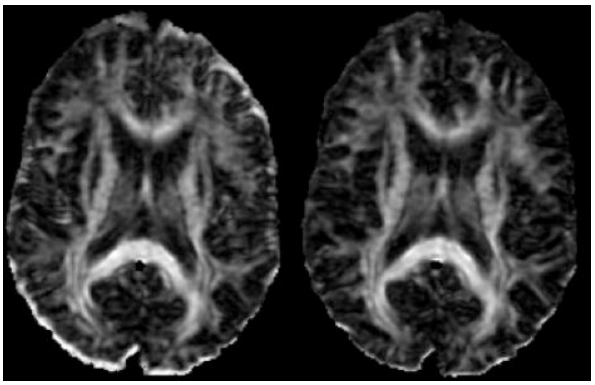

Fig. 16: Two diffusion tensor images which illustrate the effectiveness of the eddy current correction technique (left: without correction; right: with correction) [37]

Data quality control:

For DTI quality control, the first step is to import all images correctly. After this, a visual inspection of the DWI data is required to detect potential artifacts. DWI is sensitive to error introduced by imaging noise as a result of the acquisition sequence, magnet field strength, gradient amplitude, and slew rate as well as multichannel radio-frequency coils and parallel imaging. To obtain error free results, the noise is removed. In preprocessing, the raw data is converted into specific image formats. Eddy current distortion and head motion artifacts are corrected by image registration to the b_0 image. After this, skull stripping i.e. removing non-brain areas from the analysis is performed. This quality control or preprocessing step can be done using several software packages such as ExploreDTI, AFNI, DTIprep etc.

Reconstruction process:

After the preprocessing of data, tensor estimation at each voxel is performed. To estimate the tensor of the entire data set, at least six gradient directions are acquired. Since the diffusion tensor is a symmetric 3×3 matrix, it can be described by its eigenvalues $(\lambda_1, \lambda_2, \lambda_3)$ and eigenvectors $(\vec{\varepsilon}_1, \vec{\varepsilon}_2, \vec{\varepsilon}_3)$. At each voxel, the magnitude of diffusion is represented by the eigenvalues and the corresponding eigenvectors reflect the directions of maximal and minimal diffusion. Using the eigenvalues, the two main diffusion indices FA and MD are calculated which represent the magnitude of the diffusion process. After that, white matter pathways and connection patterns between different brain regions are obtained. This tractography process is divided in three main stages: seeding, propagation, and termination. Seeding consists of defining region of interest (ROI) and placing one or more seeds in each voxel of the ROI. During

propagation, fiber generation and tracking is performed with different algorithms divided in two main categories: deterministic and probabilistic. In deterministic tractography, the data are modeled to generate or reconstruct one fiber from each seed. On the other hand, for probabilistic methods, the probability maps are determined from the uncertainty of the estimation, which provides multiple possible fiber directions emanating from each seed. The last step is terminating the tracking process based on some termination criteria. These criteria aim to avoid propagating the fibers in voxels where the robustness of the vector field is not assured. The common termination criteria are minimum FA thresholds (typically 0.1 – 0.3 in adult brain and 0.1 in infant) and turning angle threshold (typically $40° - 70°$, depending on the pathway) [36].

Visualization:

To visualize the tractography result and present the tensor information in an understandable way is a big challenge. Several tools (e.g. slicer, paraview, explore DTI etc) are used to visualize the FA and MD maps and orientation distribution function of each voxel. Three dimensional WM pathways or fiber bundles are presented based on the primary eigenvector of diffusion. Using the reconstruction algorithms, 3D trajectories of fiber pathways are obtained and represented with the visualization tools. In clinical applications, the most common DTI visualization is 2D visualization of scalar maps due to its simplicity. Tools are used to show axial, coronal and sagittal views of brain in 2D and 3D.

Quantitative analysis:

This step is important to extract the information from the analysis to compare the results in different situations. It is very difficult to verify the tractography results without

ground truth data. Since the brain fiber connection structure varies from person to person and also by age of the person, it's almost impossible to have ground truth data to compare to the measured results. Currently, the parametric maps (FA and MD) are used to study specific disease processes, developmental conditions, or damaged fiber integrity in the brain. Comparing different tractography algorithm approaches gives a better understanding of white matter architecture. From the expert analysis, we can understand the positive and negative side of different tracking approaches for fiber reconstruction and get an idea of improving the tractography technique.

Generally these steps are followed to complete human brain fiber bundles tractography. In the research presented here, a dataset was obtained from St. Jude Children's Research Hospital. This dataset is described below.

3.2 Data Set

DTI was performed using an echo-planar imaging sequence on 1.5T and 3 T clinical scanners. The data sets obtained have the following characteristics:

1. 12 gradient direction 4 averages/acquisition
2. 20 gradient direction 3 averages/acquisition
3. 30 gradient direction 2 averages/acquisition
4. 64 gradient direction 2 averages/acquisition

The raw dataset (in .ima extension) cannot be used directly with the software used in this research. To make it usable for analysis, the image extension was changed to the dicom. Dicom is a software integration standard that is used in medical imaging extensively. Every dicom files holds patients information like ID, name, and data acquisition parameters (type of equipment etc). The number of dicom files in each folder is equal to

[(Number of directions + B0) * Number of averages]. Each dicom image is a composite of all N slices covering the whole brain. In the 12 direction data, the slices are 3mm thick with voxel dimension $1.8 \times 1.8 \times 3$ mm and there are 40 slices. For the 20 direction, the slices are 2 mm thick with voxel dimension $1.8 \times 1.8 \times 2$ mm and 75 slices. For the 30 direction, the slices are 2 mm thick with $1.8 \times 1.8 \times 2$ mm voxel size and 70 slices. For the 64 direction, the voxel dimension is $1.7 \times 1.7 \times 1.7$ mm where slices are 1.7 mm thick and number of slices are 96. The minimum placement of gradient field direction required to cover the whole brain is six but more directions can provide better tracking with the limitation of more time required to perform the tracking. Figure 17 shows samples of the dataset that were acquired by applying 12 and 20 gradient directions.

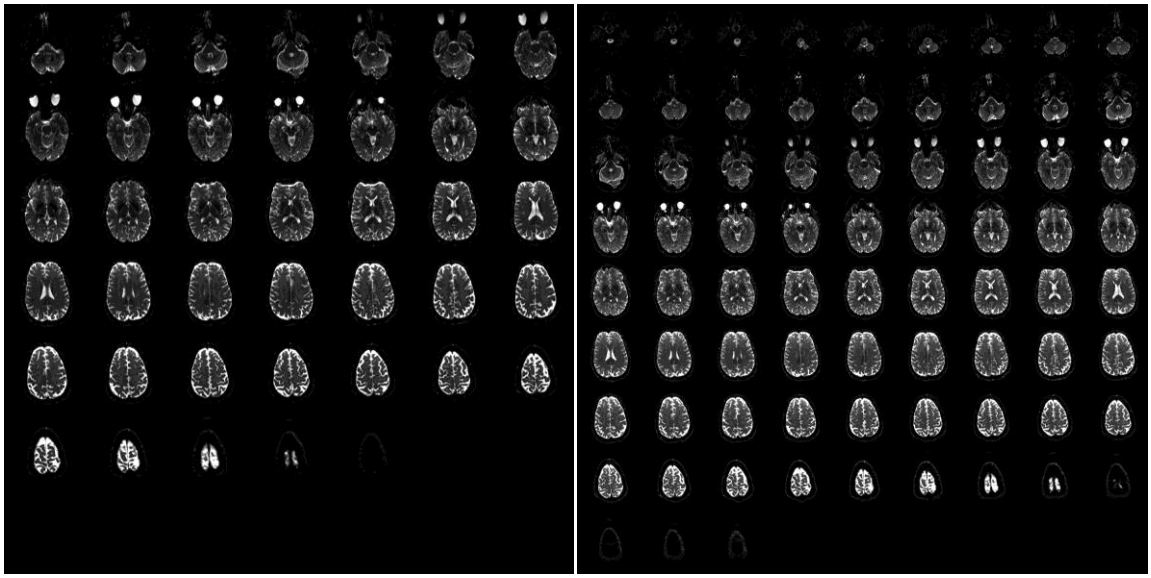

(a) (b)

Fig. 17: Dataset (a) 12 (b) 20 gradient direction

3.3 Block diagram of the tractography process used in this research:

In this research, the data acquisition step was done by researchers and staff at St. Jude Children's Research Hospital. The data was in correct order and sorted correctly. The steps followed in this research are shown in the block diagram below:

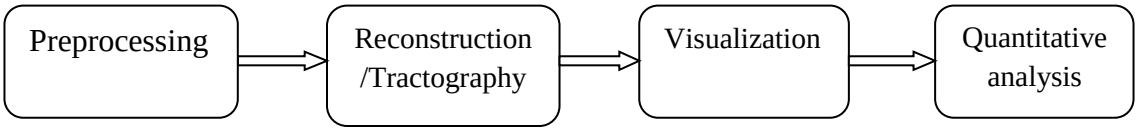

Fig. 18: Block diagram of Tractography steps

These steps are discussed in the following sections.

Pre-processing:

After data acquisition, artifacts and the quality of data are needed to be controlled. We have four set of raw data that is changed into dicom format for image analyzing. The Neuroimaging Informatics Technology Initiative (NIfTI) is a file format used in medical imaging to save fMRI data in one *.nii file. It will provide some important information like voxel dimension, orientation information (x, y, z values), b value etc. In DWI images, distortions caused by eddy current and head motion are the most common artifacts. Eddy currents can be corrected with an affine registration to the b_0 image and motion correction with a rigid body registration to b_0. After this, another step is to perform skull stripping i.e. removing non-brain areas from analysis and reducing data size [36].

Reconstruction Algorithms

This process starts by calculating diffusion tensor indices. To do so, first we need to calculate diffusion tensor. This diffusion tensor will be used to measure the fractional

anisotropy (FA), apparent diffusion coefficient (ADC), rotational anisotropy (RA) etc. for each voxel. After calculating these tensor indices, the reconstruction algorithm is applied. According to the tractography method, the reconstruction algorithm differs. In the following sections, tensor calculation method and the algorithms used for the research are discussed shortly.

Diffusion Tensor Calculation:

After preprocessing the data, diffusion tensor calculation is done. The diffusion tensor can be calculated from DWI data collected with diffusion-sensitizing gradients in six or more directions [41]. Considering six distinct tensor elements and the logarithm of the $b = 0$ signal intensity, the seven element column vector becomes:

$$\alpha = [D_{xx}, D_{yy}, D_{zz}, D_{xy}, D_{xz}, D_{yz}, \ln(S_0)]^T \tag{3.1}$$

where S_0 is the signal intensity with $b = 0$.

Each individual b matrix is represented by a six element row vector $\boldsymbol{b_i}$:

$$b_i = (b_{xxi}, b_{yyi}, b_{zzi}, 2b_{xyi}, 2b_{xzi}, 2b_{yzi}) \tag{3.2}$$

which is part of a seven element row vector $\boldsymbol{B_i}$: $B_i =$

$$(-b_{xxi}, -b_{yyi}, -b_{zzi}, -2b_{xyi}, -2b_{xzi}, -2b_{yzi}, 1) \tag{3.3}$$

The row vectors are combined into one large $N \times 7$ **B** matrix:

$$\boldsymbol{B} = \begin{pmatrix} -b_{xx1} & -b_{yy1} & -b_{zz1} & -2b_{xy1} & -2b_{xz1} & -2b_{yz1} & 1 \\ \vdots & \vdots & \vdots & \vdots & \vdots & \vdots & \vdots \\ -b_{xxN} & -b_{yyN} & -b_{zzN} & -2b_{xyN} & -2b_{xzN} & -2b_{yzN} & 1 \end{pmatrix} \tag{3.4}$$

Without noise, the logarithms of the predicted signal intensities are given by a $N \times 1$ column vector ξ:

$$\xi_i = \boldsymbol{B}_i\alpha = \ln(S_i) = \ln(S_0) - b_i{:}\,\boldsymbol{D}$$

$$\xi_i = -b_{xxi}D_{xx} - b_{yyi}D_{yy} - b_{zzi}D_{zz} - 2b_{xyi}D_{xy} - 2b_{xzi}D_{xz} - 2b_{yzi}D_{yz} + \ln(S_0) \tag{3.5}$$

So, the generalized dot product between the **b** matrix and the diffusion tensor **D** becomes

$$b_i{:}\,\boldsymbol{D} = b_{xxi}D_{xx} + b_{yyi}D_{yy} + b_{zzi}D_{zz} + 2b_{xyi}D_{xy} + 2b_{xzi}D_{xz} + 2b_{yzi}D_{yz} \tag{3.6}$$

$$\xi = \boldsymbol{B}\alpha$$

$$= \begin{pmatrix} -b_{xx1}D_{xx} - b_{yy1}D_{yy} - b_{zz1}D_{zz} - 2b_{xy1}D_{xy} - 2b_{xz1}D_{xz} - 2b_{yz1}D_{yz} + \ln(\mathrm{S}_0) \\ \vdots \\ -b_{xxN}D_{xx} - b_{yyN}D_{yy} - b_{zzN}D_{zz} - 2b_{xyN}D_{xy} - 2b_{xzN}D_{xz} - 2b_{yzN}D_{yz} + \ln(S_0) \end{pmatrix}$$

The noisy observed data are represented by a $N \times 1$ column vector **x:**

$$\boldsymbol{x} = \begin{pmatrix} ln(S_1) \\ \vdots \\ \ln(S_N) \end{pmatrix} \tag{3.7}$$

The noisy data for each acquisition can be expressed as

$$\boldsymbol{x} = \boldsymbol{B}\alpha + \boldsymbol{\eta} = \boldsymbol{\xi} + \boldsymbol{\eta} \tag{3.8}$$

where $\boldsymbol{\eta}$ is a noise vector. If we set $\eta = 0$, the solution of the true tensor α becomes [41]:

$$(\boldsymbol{B^{-1}B})\alpha = \alpha = \boldsymbol{B}^{-1}\boldsymbol{x} \tag{3.9}$$

With exactly six directions, the six measured ADCs can be found from the gradient scheme in the following Table. The ADCs are given by [41]-

$$D_1 = \frac{(D_{xx} + 2uD_{xy} + u^2 D_{yy})}{(1 + u^2)}$$

$$D_2 = \frac{(D_{xx} - 2uD_{xy} + u^2 D_{yy})}{(1 + u^2)}$$

$$D_3 = \frac{(D_{yy} + 2uD_{yz} + u^2 D_{zz})}{(1 + u^2)}$$

$$D_4 = \frac{(D_{yy} - 2uD_{yz} + u^2 D_{zz})}{(1 + u^2)}$$

$$D_5 = \frac{(D_{zz} + 2uD_{xz} + u^2 D_{xx})}{(1 + u^2)}$$

$$D_6 = \frac{(D_{zz} - 2uD_{xz} + u^2 D_{xx})}{(1 + u^2)}$$

$$D_{av} = \frac{(D_1 + D_2 + D_3 + D_4 + D_5 + D_6)}{6} = \frac{D_{xx} + D_{yy} + D_{zz}}{3} \quad (3.10)$$

For the polyhedral encoding schemes with any value of the tensor element u, the b matrix can be calculated from the following table 1.

Once we calculate the mean diffusivity, other diffusion indices can be easily calculated using the value of D_{av}.

Table 1: Calculation of the b Matrix for a Common Six-Direction DTI Gradient-Encoding Scheme [43]

g_x	g_y	g_z	b_{xx}	b_{yy}	b_{zz}	b_{xy}	b_{xz}	b_{yz}
1	u	0	1	u^2	0	u	0	0
1	$-u$	0	1	u^2	0	$-u$	0	0
0	1	u	0	1	u^2	0	0	u
0	1	$-u$	0	1	u^2	0	0	$-u$
u	0	1	u^2	0	1	0	u	0
$-u$	0	1	u^2	0	1	0	$-u$	0

Originally fractional anisotropy (*FA*) ranged from 0 to 1, relative anisotropy (*RA*) from 0 to $2^{1/2}$, and volume ratio (*VR*) from 1 to 0. The formula for calculating these indices in terms of tensor elements are given by:

$$\text{Fractional anisotropy, } FA = \sqrt{\frac{3[(D_{xx}-D_{av})^2+(D_{yy}-D_{av})^2+(D_{zz}-D_{av})^2+2(D_{xy}^2+D_{xz}^2+D_{yz}^2)]}{2[D_{xx}^2+D_{yy}^2+D_{zz}^2+2(D_{xy}^2+D_{xz}^2+D_{yz}^2)]}} \quad (3.11)$$

$$\text{Relative anisotropy, } RA = \sqrt{\frac{(D_{xx}-D_{av})^2+(D_{yy}-D_{av})^2+(D_{zz}-D_{av})^2+2(D_{xy}^2+D_{xz}^2+D_{yz}^2)}{3D_{av}^2}} \quad (3.12)$$

$$\text{Volume Ratio, } VR = \frac{1-[D_{xx}D_{yy}D_{zz}+2D_{xy}D_{xz}D_{yz}-(D_{zz}D_{xy}^2+D_{yy}D_{xz}^2+D_{xx}D_{yz}^2]}{D_{av}^3} \quad (3.13)$$

The tractography methods used in this thesis are discussed in the following sections.

Deterministic tractography: FACT

Fiber assignment by continuous tracking (FACT) algorithm is a time and memory effective three-dimensional tract reconstruction method. It is a deterministic tractography process that uses a brute-force reconstruction approach. In this method, tracking is performed using a continuous coordinate system rather than a discrete voxel-based matrix grid. The tracking is started at the center of each voxel having FA value greater than a user-defined threshold and proceeds along the principle eigenvector direction [40]. Tracking direction is changed at the point where the track intercepts the voxel's boundary. To find the interception point, the 3D space fiber track within the voxel is parameterized by arc length s, and expressed by

$$\begin{cases} x = x_0 + v_x s \\ y = y_0 + v_y s \\ z = z_0 + v_z s \end{cases} \tag{3.14}$$

Where $\boldsymbol{v} = (v_x, v_y, v_z)$ is the principle eigenvector and $x_0 = (x_0, y_0, z_0)$ is the starting point where the fiber track enters the voxel and $\boldsymbol{x} = (x, y, z)$ is the interception point.

The solution of the equation is the minimum s that makes x, y, or z in this equation a constant. After getting the interception point in the boundary, the direction of new vector is found by taking an inner product between current and the new vector. If the result is negative, swap sign of the new vector. To get the complete trajectory, tracking is continued in both forward and backward directions initiated from the seed voxel. The tracking process is stopped if the angle between current direction and new direction is greater than the set threshold and to avoid shorter tracts than a threshold, minimum fiber length testing is subsequently performed. The end of the projection is judged based on sudden transitions in the fiber orientation and the transition is quantified by-

$$R = \sum_i^s \sum_j^s abs(v_{\lambda 1i} \cdot v_{\lambda 1j})/s(s-1) \quad (3.15)$$

Where $v_{\lambda 1}$is the unit vector representing the longest principle diffusion axis and s is the number of data points referenced. When adjacent fibers are aligned strongly, the *R* value is large, while it becomes small in regions without continuity in fiber direction [38].

In a particular region of interest (ROI), the tracking may meet a branching point which would be forced to follow a single point of them. Brute-force fiber tracking is used to solve this situation.

Probabilistic Tractography: PICo

Probabilistic methods utilize the probability density function (PDFs) of each point within the brain to describe the local uncertainty in fiber orientation. Each PDF interpret the diffusion imaging acquisition information in terms of the likely underlying fiber structure. To interpret the diffusion tensor for probabilistic connectivity analyses, two orders of uncertainty are introduced. In 0^{th} order case, uncertainty in the v_x orientation is defined by tensor anisotropy, providing an isotropic normal distribution of orientation. In the 1^{st} order case, the orientations of v_y and v_z and their respective eigenvalues provide orthogonal directional uncertainties, thus providing a more accurate bi-normal distribution of orientation [34].

To calibrate the PICo PDF by adding noise to synthetic data, the parameters of the PDF is fitted to the fiber orientation estimates. A zero mean Gaussian model for the diffusion displacement density $p = G(D, t)$ in each voxel, where D is the diffusion tensor and t is the diffusion time, is considered to produce a look up table with different diffusion tensors that maps tensor anisotropy to PDF concentration. For two fiber bundles in a voxel, a Gaussian mixture model is fitted. For each noisy set of measurements, a

Gaussian mixture model: $p = \alpha G(D_1, t) + (1 - \alpha)G(D_2, t)$, where diffusion tensors are identically anisotropic, cylindrically symmetric and orthogonally oriented, is considered. In a similar way, two spherical PDFs of Bingham distribution [35]:

$$f(\pm x) = B(\pm x;\ \kappa_1, \kappa_2, \mu_1, \mu_2) = M^{-1} \exp[\kappa_1(\mu_1^T x)^2 + \kappa_2(\mu_2^T x)^2], \quad \kappa_1 < \kappa_2 \leq 0, \tag{3.16}$$

where the axes μ describes the orientation of the distribution, κ describe the concentration and M is a constant, are fitted to the fiber orientation estimates $x_1 \ldots \ldots x_{2N}$.

Given the sample of fiber orientations, the maximum [35]

$$L = \sum_{i=1}^{2N} 0.5B(x_i; \kappa_1, \kappa_2, \mu_1, \mu_2) + 0.5B(x_i; \kappa_3, \kappa_4, \mu_3, \mu_4) \tag{3.17}$$

with respect to the orientations and concentration of the two Bingham PDFs is found.

A step in the streamline propagation process is defined by-

$x(l + 1) = x(l) + w(l)\delta t$, where $x(l)$ is the position in $\Re^3$ of the streamline at point l on its length, $w(l)$ is the propagation direction at this point ($l \rightarrow x$), and δt is the step size. With a single tensor model of diffusion, $w(l)$ is defined as the interpolated principle diffusion direction (PDD) at that point. PDD is determined by tri-linear interpolation of surrounding tensor elements. If one or more image voxels are involved in the interpolation, the selected tensor satisfies,

$$\max_i(\left|\Gamma\big(D_i(p)\big) \cdot w(l-1)\right|)$$

where $\Gamma\big(D_i(p)\big)$ is the PDD of the i^{th} tensor at image location p. This formulation ensures further streamline propagation in case of fiber crossing.

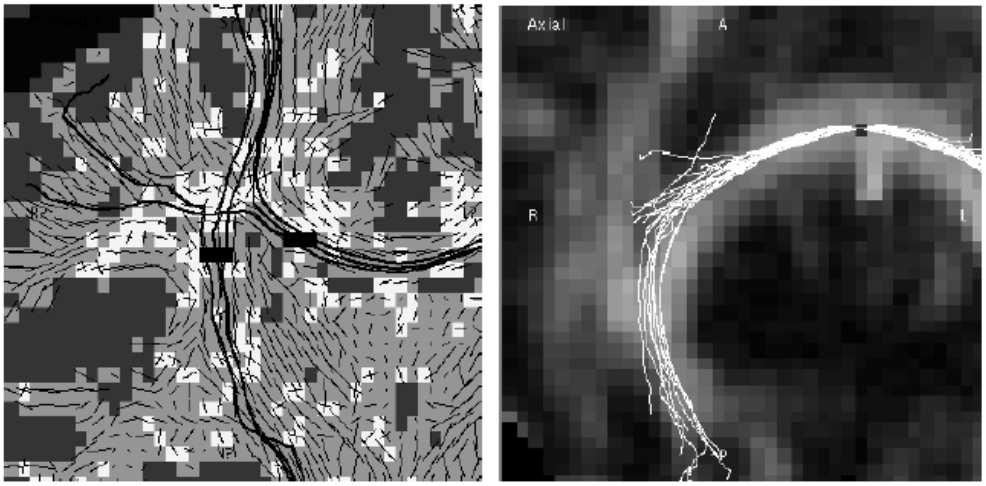

(a) (b)

Fig. 19: (a) streamline propagation (black continuous lines) through a region of crossing fibers (b) Illustration of streamline randomization process in the corpus callosum [33]

The PICo method utilizes Monte Carlo streamline approach, sampling the orientation PDFs within each voxel on each iteration.

To define a map of the probability, ψ, of connection to the start point, is given as $\psi(p) = \lim_{N\to\infty} \frac{\mu(p,N)}{N} \approx \frac{\mu(p,N)}{N}$ where $\mu(p,N)$ represents number of occasions over N repetitions at each voxel p is crossed by a streamline [33].

Gibbs Tracking:

This is a global tractography method that can reconstruct crossing and spreading fiber configurations without interpolation or strong a priori constraints. In this method, the fibers are built with small line elements. Each line element contributes an anisotropic term to the simulated DW signal, which is adjusted to the measured signal. The process started at high temperature (time parameter of simulated annealing method), which is slowly decreased during the simulations to ensure the independence of the initial state

and to find the optimal configuration. This process is named as Gibbs tracking" which is actually a Bayesian approach, based on spatial point processes [39]. According to this, the interaction between the cylinders represents the a priori probability and likelihood function is determined by the similarity between the measured and the simulated signals. The Gibbs tracking method defines the neuronal pathways by small cylinders. Each cylinder is defined by the tuple $h_i = (r_i, m_i)$ where $r_i = (x_i, y_i, z_i)$ specifies the center of the cylinder and $m_i = (l_i, \theta_i \emptyset_i)$ defines the length, polar angle and azimuth angle respectively. The radius for all cylinders is identical. The two ends a_i^+ and a_i^- of the cylinder h_i are calculated by equation 3.18 and 3.19:

$$a_i^+ = r_i + \frac{l_i}{2}\begin{pmatrix} cos\ \emptyset_i\ cos\ \theta_i \\ sin\ \emptyset_i\ cos\ \theta_i \\ -sin\ \theta_i \end{pmatrix} \tag{3.18}$$

$$a_i^- = r_i - \frac{l_i}{2}\begin{pmatrix} cos\ \emptyset_i\ cos\ \theta_i \\ sin\ \emptyset_i\ cos\ \theta_i \\ -sin\ \theta_i \end{pmatrix} \tag{3.19}$$

To differentiate between the white matter and the gray matter, there are predefined border planes which are aligned to the grid and lie on the border surface of two neighboring voxels. The probability of a given configuration of cylinders, $\omega = \{h_1, \ldots \ldots h_n\}$ is defined in the form: $f_T(\omega) = \exp\left(-\frac{1}{T}U_I(\omega)\right)\exp\left(-\frac{1}{T}U_D(\omega, \hat{S})\right)$ (3.20)

where U_I represents the interaction energy and U_D corresponds to the data energy and T is the overall temperature of the system. In the equation, the potential function $f_T(\omega)$ can be seen as a non-normalized a posteriori probability at the temperature T, $\exp(-\frac{1}{T}U_I(\omega))$ defines the a priori probability and $\exp(-\frac{1}{T}U_D(\omega, \hat{S}))$ defines the likelihood function.

The interaction energy favors the formation of the cylinders into chain i.e. neuronal pathways and data energy depends on the difference between the measured signal with the simulated one to determine the likelihood.

The interaction energy is expressed in terms of the number of cylinders in different states defined according to their position relative to other cylinders and boundaries. In the attraction area, two endpoints are attracted with the energy

$$g_{attr}(a_i, a_j) = 1 - \left(1 - \frac{\left(d_{attr} - \|a_i - a_j\|_\infty\right)^q}{(d_{attr} - d_{con})^q}\right)^{\frac{1}{q}} \tag{3.21}$$

Here q is a predefined constant, influencing the shape of the potential function. The interaction is switched off if one of the endpoints is connected. So, the interaction energy takes the form:

$$U_I(\omega) = w_f N_f(\omega) + w_s N_s(\omega) - w_a W_a(\omega) + w_w N_w(\omega) \tag{3.22}$$

where the terms w_f, w_s, w_a and w_w are positive weights that influence the priority of different criteria and N_f, N_s and N_w are the numbers of free, single connected and wrongly connected cylinders respectively.

The formula for calculating data energy is

$$U_D(\omega) = u \sum_{x \text{ in } WM} \sum_{k=1}^{I} [\left(\hat{S}_k^*(x, \omega) - \overline{\hat{S}_k^*(x, \omega)}\right) - \left(\hat{S}_k(x) - \overline{\hat{S}_k(x)}\right)]^2 \tag{3.23}$$

Here $\hat{S}_k(x)$ and $\hat{S}_k^*(x, \omega)$ are the measured and simulated signals, respectively.

To maximize the a posteriori probability $f_T(\omega)$, a reversal jump Monte Carlo Markov chain (RJMCMC) combined with the simulated annealing can be used. In this method the

last configuration ω_J after reaching the final temperature T_J is used as a result. If we consider a series of configuration $(\omega_0, \dots, \omega_t, \omega_{t+1}, \dots)$ according to a given probability density function, $f_T(\omega)$, the configurations form a chain of points in the state space Ω where the next element depends only on its predecessor.

After completing tractography, we need to visualize the results. Visualization and the quantitative analysis of the results will be discussed in the next chapter. From the quantitative analysis, DTI provides information about a healthy and a diseased brain. For an example, DTI has been used to differentiate low-grade to high-grade brain tumors and its consequences. The change of FA between lesion and contralateral hemispheres distinguishes the WM tracts due to brain tumors as edematous, displaced, infiltrated and disrupted [42]. The FA change is defined by

$$\Delta FA_{\%} = \frac{FA_{lesion} - FA_{normal}}{FA_{normal}} \times 100\% \tag{3.24}$$

If $\Delta FA_{\%}$ is less than -30%, it is likely to be associated with WM disruption which means anisotropy is markedly reduced resulting at least partially destroyed WM tracts. A positive $\Delta FA_{\%}$ indicates edema or displacement and a $\Delta FA_{\%}$ between 0% to -30% is associated with Wm displacement or infiltration. WM integrity remains unaffected due to this alteration of FA values near brain tumors. In summary, DTI can assess white matter tract integrity and organization in the brain both in normal and disease case.

CHAPTER 4

SIMULATION RESULTS

In this chapter, I have reported about the simulation steps, tools used for various processing and the results of fiber bundles tracking for all the techniques. The simulations are done in three steps:

1. Pre-processing
2. Diffusion indices calculation
3. Tractography

First two steps are common for both deterministic and probabilistic methods. After calculating the diffusion indices, FACT, PICo and Gibbs tracking algorithm are used to reconstruct the fiber paths. The steps are described below.

4.1 Pre-processing

The dataset is converted from *.ima format to *.dicom for image analysis. Every dicom file holds patient information including ID, name, and data acquisition parameters (type of equipment etc). After getting the data in correct order, the artifacts due to head motion and eddy currents are removed. Deterministic and probabilistic tractography are performed using “Camino” [44]. It is an open source software toolkit for diffusion MRI processing. Three files are required to start the tractography using Camino. They are:

(i) A raw DWI data in Neuroimaging Informatics Technology Initiative (NIfTI) format

(ii) List of gradient directions and

(iii) Brain mask in NIfTI format separating brain from the background.

Eddy current correction:

In this process, affine registration to the b_0 image is done to correct the eddy current artifacts. Figure 20 shows a sample of eddy current correction by affine registration. Here, the second row shows the distorted images which are corrected by taking b_0 images as a reference (first row) and following the affine transformation (third row). This step is done using "SPM8" [52].

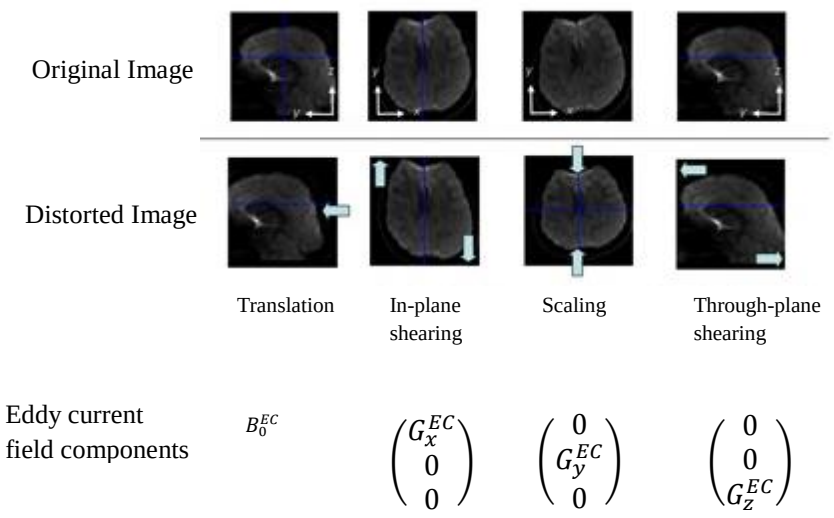

Fig. 20: Sample of eddy current correction [51]

Dicom to NIfTI conversion:

The NIfTI is a file format used in medical imaging to save fMRI data in one *.nii file. It provides some important information like voxel dimension, orientation information (x,y,z values or gradient directions), b value etc. The registered dicom images are converted to NIfTI using "MRIcron" [49] software.

Gradient directions are saved in a text file as given in the appendix A for 12 directions 4 averages data set. In the text file, each subsequent line represents a separate image in the protocol and the order is the same as the order in which the images are acquired. If the b-value is zero, the gradient direction does not matter so it is set $x = y = z = 0$ in the text file. The other images are acquired with b-value 1000 s/mm^2.

Creating brain mask:

Skull stripping or removing non-brain areas using "BrainSuite" [47] is shown in Fig. 21. It operates using an edge detector to find a boundary between brain and the skull. The detection continues up to some threshold (for example the threshold was 180 for 12 direction data set brain mask) and morphological operators are used to provide better separation of the tissue. Before the edge detection performs, an anisotropic diffusion filter is applied to sharpen the high contrast edges and blur the low contrast edges.

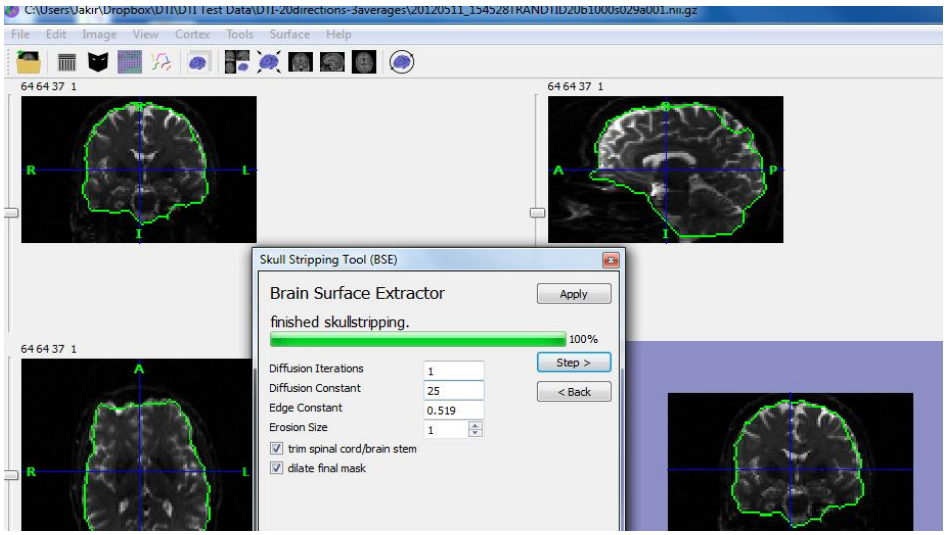

Fig. 21: Skull-stripping using BrainSuite.

4.2 Diffusion indices calculation:

When the above three files are ready, a scheme file that lists the details of the acquisition is generated. Next the DWI data is fitted to each voxel. Once the data is in voxel order, it can be easily split up (e.g. by slice) and processed in parallel. Voxel-based single and multi diffusion tensor models for the orientation distribution function (ODF) are fit to the data by Camino as shown in Fig. 22. After calculating D_{av} and FA using equation 3.10 and 3.11 respectively, the orientation distribution function (ODF) is obtained. It is then used to describe the directionality of multimodal diffusion in regions with complex fiber architecture present in the brain. The maximum diffusivity is normalized to voxel size. The color indicates the direction of maximum diffusivity i.e. red means left to right, green indicates anterior-posterior and blue for superior-inferior.

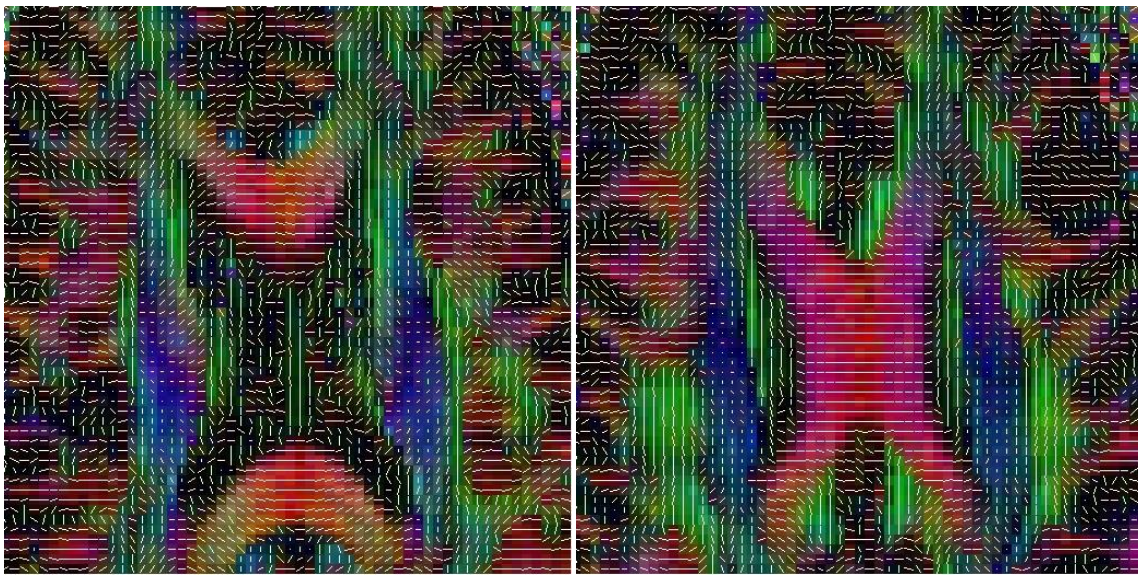

Fig. 22: Orientation distribution function (ODF) for slice no. 44 and 47 in a 20D data set.

4.3 Tractography

The tractography process is done in three steps: select a region of interest (ROI), tracking fibers, and visualization of the connections.

Selecting a region of interest:

To initialize the tracking, a seed point from where the tracking will be started is selected manually. Seed point is chosen from a defined region of interest (ROI). The ROIs can be manually drawn or extracted from other MRI modalities. Here, ROI has been selected by "ITK snap" [48] tool.

Corpus callosum (CC) is the largest white matter structure in the brain. It connects the left and right cerebral hemispheres. Selecting CC as an ROI will give a maximum number of fiber connections. To track through the diffusion data, the seed points initiate streamlines and the CC is defined as an ROI in the FA map manually.

Tracking fibers and visualization:

FACT: The selected ROI and some thresholds for Camino are used for FACT simulation. The thresholds, for example, set the angle threshold 60° and anisotropic threshold 0.2. These threshold values specify that tracks are terminated when anisotropy falls below 0.2 and the angle between 2 diffusion directions in adjacent voxel is larger than 60°. During the tracking process, the fibers are gradually generated.

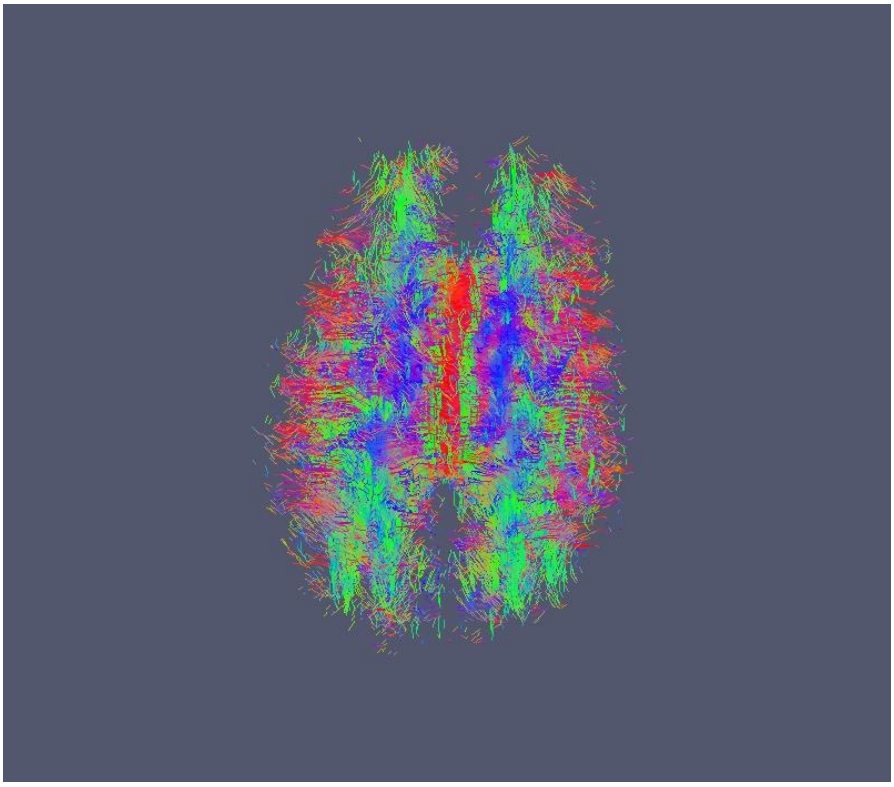

Fig. 23: Deterministic tractography of 12 directions 4 averages data set using Camino.

Fiber connections are visualized using the “Paraview” [45] tool. Figure 23 shows fiber connections for a 12 direction data set in axial view. Deterministic tractography models the data to generate/reconstruct one fiber from each seed.

PICo: For probabilistic tractography, Camino can track streamlines using Bayesian tractography and PICo tractography algorithms. In my work, I used the PICo algorithm because Bayesian tractography is more data driven and doesn’t generalize easily to multiple fiber orientations. In PICo technique, a probability density function is computed for each voxel. The probability density functions (pdfs) are calculated from a lookup table which is generated for a certain signal to noise ratio (SNR). The seed ROI is used to generate the probabilistic tracked streamlines by iteration.

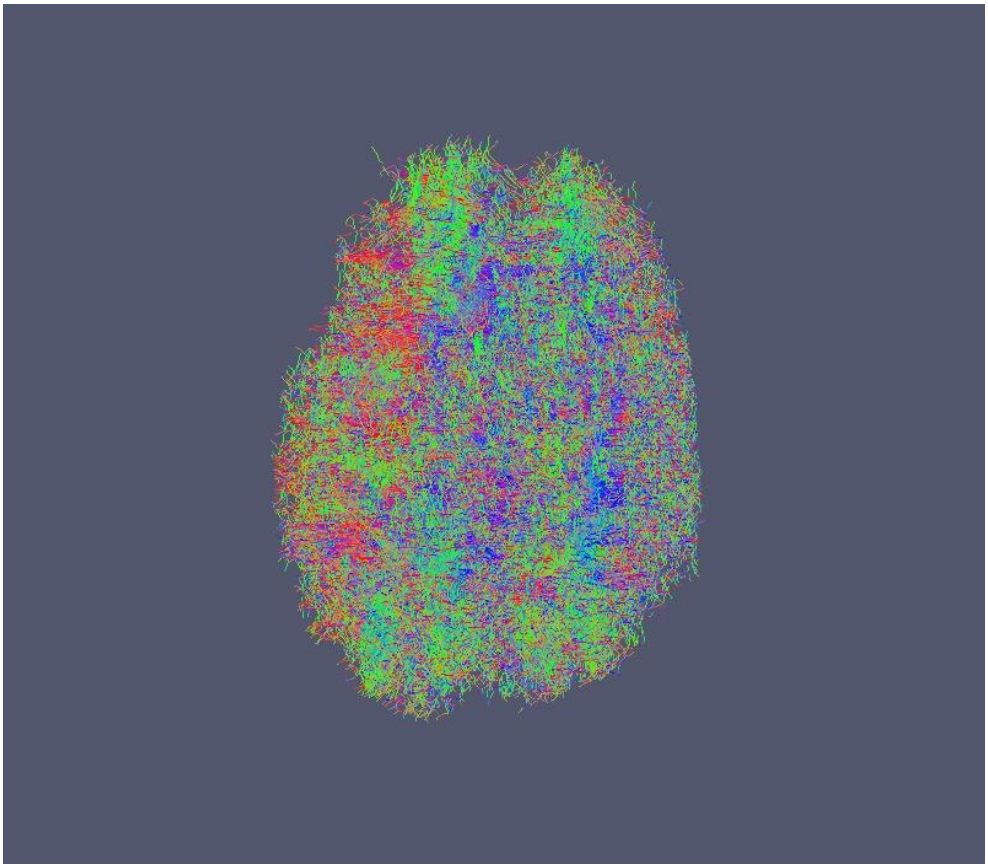

Fig. 24: Probabilistic tracking of 12 direction data set.

The reconstructed fibers are again visualized in the Paraview tools. Figure 24 is showing tractography result of a 12 directions data set for probabilistic tracking and shows a higher density of fibers than the deterministic process.

Gibbs tracking: For Global tractography, I have used DTI & Fiber tools [50] to simulate Gibbs tracking technique as shown in Fig. 4.6. This tool not only is used for simulating Gibbs tracking but also for FACT and PICo. Therefore the results obtained using this help to compare the methods. Here, the calculated tensors are saved in 'dtdStruct' form, which consist the information of the eigenvalues, eigenvectors and the mean of the b_0 images.

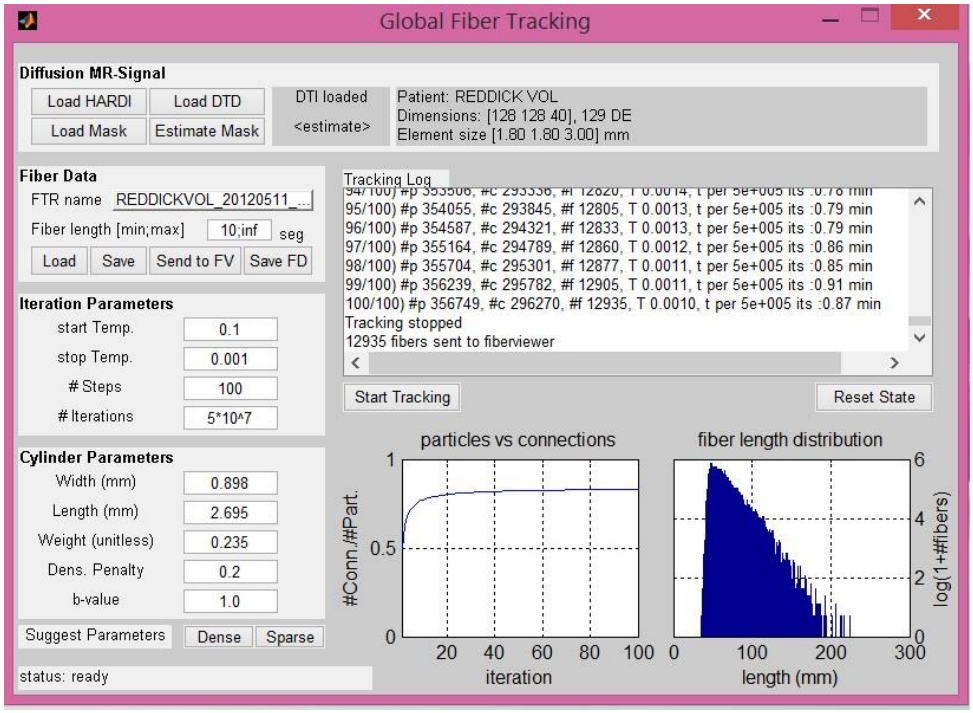

Fig. 25: Simulation of Gibbs tracking

To start Gibbs tracking for global tractography, diffusion tensor information and a brain mask are provided as inputs for simulation. There are two types of parameters that are controlled for better reconstruction. Cylinder parameters of the fiber model and parameters concerning the iteration process are set manually. The cylinder parameters, including length and width, are set. The iteration parameters which include the starting and stopping temperature with the number of iterations are set. The values for all the parameters are shown in Fig. 25 as set for the simulation. The computation time and memory required for Gibbs tracking is very high. For this work, Intel PC core i5, 2.5 GHz, 8.0 GB RAM windows 8 as an operating system and high power computing (HPC) having 512 GB RAM is used and it takes 12-24 hours for completing the simulation. But the computation time for FACT and PICo is short; not more than 1 hour which is the main advantage of these two methods. The stopping criteria for FACT tracking is $FA \leq$

0.2 and maximum angular threshold 60°. For PICo, it is limited to visit maximum 150 voxels and the simulation stops if $FA \leq 0.2$.

Figure 26 and 27 are showing tractography of the whole brain and the fiber paths in a single slice of the brain for 12 and 30 direction data sets.

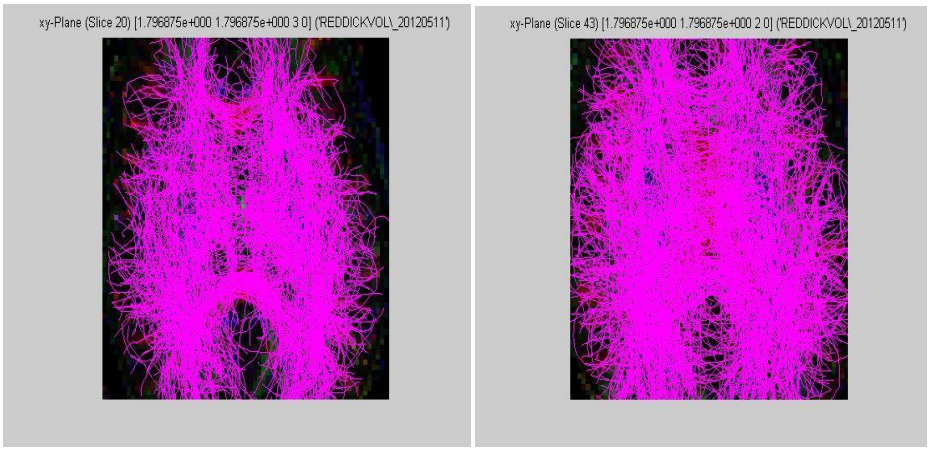

(a) (b)

Fig. 26: visualization of tractography using Gibbs tracking (a) 12 D (b) 30 D

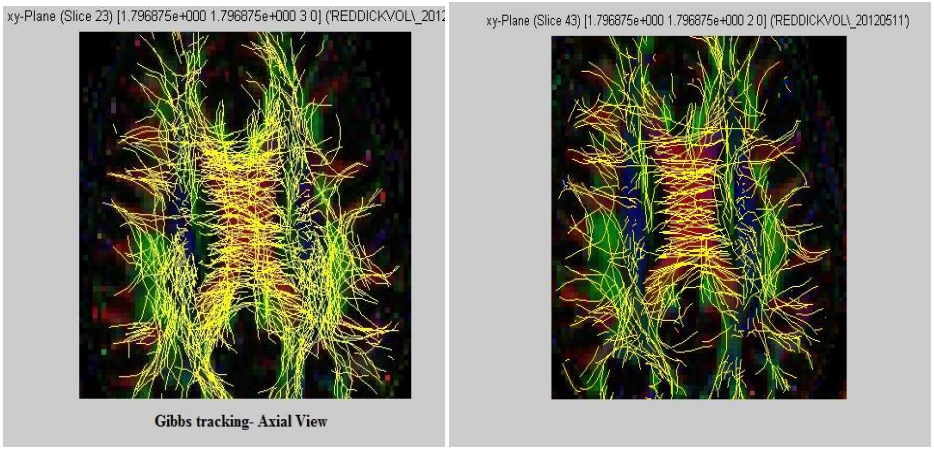

(a) (b)

Fig. 27: visualization of tractography in single slice using Gibbs tracking (a) 12D (b) 30D

4.4 Comparison

Handling crossing and kissing:

Fiber crossing and kissing is visualized by fitting multi-tensor model to each voxel. In Fig. 28, ODF for both single and multi tensor model in a 64 direction data set is shown where the overlapping of two tensors indicates kissing and crossing fibers in Fig 28(b).

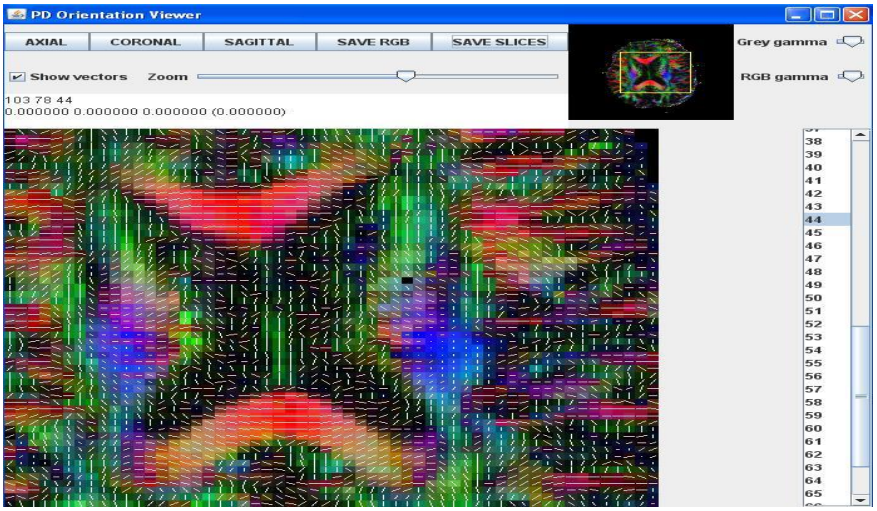

(a)

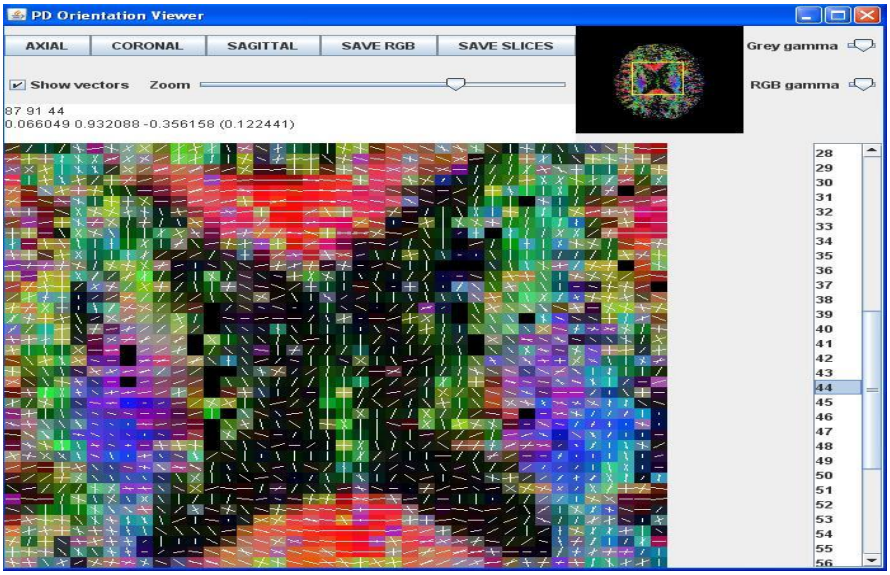

(b)

Fig. 28: ODF by applying (a) single tensor (b) multi tensor model in a 64 D data set

In deterministic tractography (FACT), the algorithm is forced to take any one tensor's principle direction and adds sequentially each voxel to construct the fiber path, which may differ from the exact path. A single mistake in deciding the tensor connections when crossing and kissing exist in a voxel may mislead the total fiber pathway tracking. It is a major limitation of deterministic tractography which is overcome by the probabilistic approach. In the probabilistic approach (PICo), the pdf of the multi-tensor in each voxel is used to find the most likely path to connect sequentially. Gibbs tracking can handle the crossing and kissing fibers more effectively. It reconstructs the fibers by measuring the pdf of the whole fiber pathway. The performance of all these tractography techniques in crossing and kissing fibers tracking are compared on the basis of single slice visualization and the mean length of fibers reconstructed in the following section.

Fibers reconstruction:

Figure 29 and 30 are showing the comparison of fiber connections for the same slice (slice no. 23) and plane in three different views of brain: axial, sagittal and coronal using 12 direction data set for FACT, PICo and Gibbs tracking.

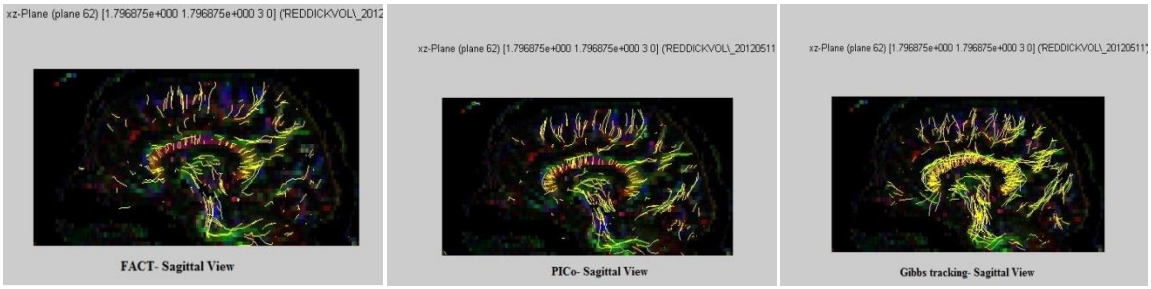

Fig. 29: Fiber connections for FACT, PICo and Gibbs tracking from Sagittal view of brain using 12 D data set

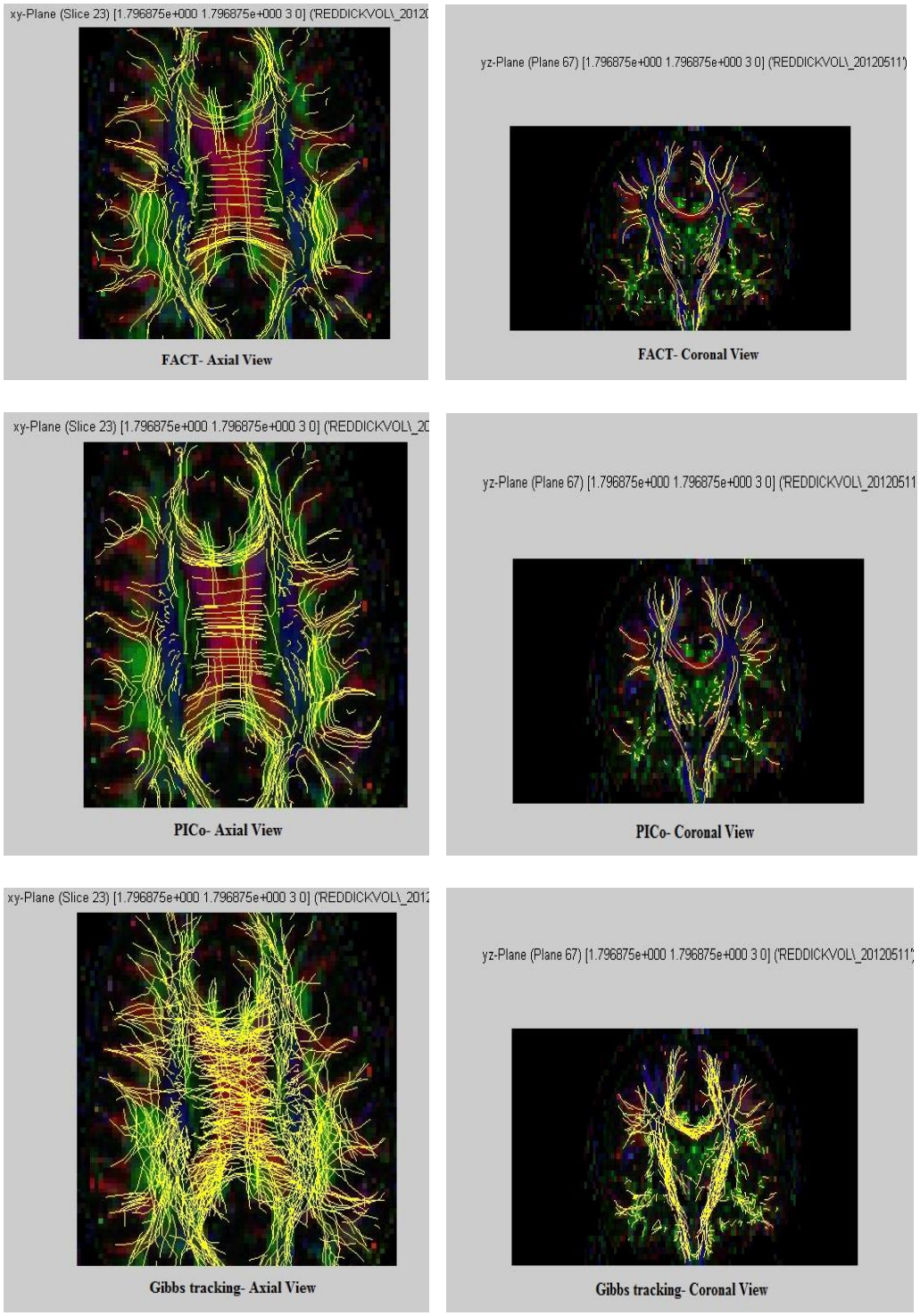

Fig. 30: Fiber connections for FACT, PICo and Gibbs tracking from axial and coronal view of brain using 12 D data set

From the figures, it can be seen that the fiber numbers or densities are highest in Gibbs tracking whereas the lowest number of fibers is found from the FACT algorithm. The mean length of fibers tracked during the reconstruction process for all three tractography approaches are listed in table 2. From the table, the mean length of fibers tracked in Gibbs tracking is greater than other two approaches for each data set which indicates better performance of Gibbs tracking. But compare to deterministic approach, probabilistic tractography can reconstruct higher length of fibers. The table also indicates that the mean length of fibers increased with an increment in the number of gradient directions.

Table 2: Comparison of mean length of fiber for different tractography approach

Directions	Mean length of fiber (mm)		
	Deterministic Approach (FACT)	Probabilistic approach (PICo)	Gibbs tracking
12	35.3032	53.7876	72.2315
20	32.9716	55.3511	79.9543
30	37.0210	77.5026	86.5967
64	38.2012	78.1388	86.1916

Statistical Comparison:

For comparing the tractography approaches statistically, paired t-test is performed using four set of datasets for greater sensitivity. From table 2, after performing the paired t-test between deterministic (FACT) and probabilistic tractography (PICo), I obtained $t =$

5.2590 and $P = 0.0135$. Consider the standard t-table of significance as given in table 3 using two-tails hypothesis for degree of freedom, $df = 3$.

Table 3: Standard t-table for two-tails hypothesis with different significance level, α [53]

$t \rightarrow$ $\alpha \rightarrow$	$t_{0.90}$ 0.2	$t_{0.95}$ 0.1	$t_{0.975}$ 0.05	$t_{0.99}$ 0.02
$df = 2$	1.886	2.9199	4.3026	6.965
$df = 3$	1.638	2.3533	3.1824	4.541

So comparing $t = 5.2590$ and $P = 0.0134$ with table 3, it can be said that it rejects the null hypothesis. It indicates that there is statistically significant difference between the means of two methods: FACT and PICo. As per table 2, since the mean length of fibers in PICo for every data set is greater than FACT tracts mean length, it can be said that PICo is better than FACT. Similarly, comparing the FACT and Gibbs tracking using paired t-test, I got $t = 15.8422$ and $P = 0.0005$. From table 3, it also rejects the null hypothesis. From these two paired t-tests, it is clear that t-value for FACT and Gibbs tracking test is higher than FACT and PICo test. So, it can conclude that Gibbs tracking provides higher mean length of fibers than other two methods and deterministic tractography determines the smallest mean length of fibers. But the result would be more reliable from the statistical point of view if we can run simulation on more MRI data sets.

4.5 Clinical application of tractography

From the tractography process, I calculate different diffusion indices which are used to differentiate between a healthy and a diseased brain. I have data sets of three patients' who went through radiation therapy (RT) after brain tumor surgery. The data set contains two parts: before RT and after RT. Simulating the data sets, I can quantify the changes due to radiation therapy as given in the table 4 and 5. Table 4 indicates two important indices of tractography FA and ADC for different data sets. These values are taken from selecting a particular region of interest (ROI) near to CC. Considering the mean of each index, there is some differences in the values between the pre and post radiation therapy of every data set. The mean length of fibers is also quantified in table 5. So the change of indices and fiber length indicates a variation due to radiation therapy in a patient's brain.

Table 4: Comparison of pre and post radiation therapy (RT) effect

Patients No.	Pre/post RT	Mean FA	Mean ADC
1	Pre RT	7.694×10^{-1}	1.006×10^{-3}
	Post RT	7.590×10^{-1}	0.931×10^{-3}
2	Pre RT	7.081×10^{-1}	1.143×10^{-3}
	Post RT	8.174×10^{-1}	0.843×10^{-3}
3	Pre RT	7.665×10^{-1}	0.904×10^{-3}
	Post RT	6.488×10^{-1}	1.034×10^{-3}

Table 5: Mean length of fibers comparison between pre and post RT datasets

Patients/Datasets [64 Directions 2 Averages]	Mean length of fibers in mm	
	Before/pre radiation therapy	After/post radiation therapy
1	76.4938	79.2784
2	83.3513	80.1393
3	71.8039	70.5212

FA and ADC values can be used to characterize diseased areas of the brain e.g. to detect the WM tracts adjacent to brain tumors to determine a viable tract. This will help to determine whether a specific region should be kept or resected during surgery. It also specifies patient information how much he/she recovered from a disease after surgery.

Statistical Comparison of RT effects:

The FA and ADC values along with mean length of fibers indicate that due to radiation therapy some changes occur in the brain after the therapy. A statistical analysis using paired t-test is applied to determine how the variation is statistically significant. From table 4, after performing the paired t-test between pre and post RT mean FA values, I got $\mathrm{t} = 0.0956$ and $\mathrm{P} = 0.9326$. Similarly comparing mean ADC values between pre and post RT, the value of $\mathrm{t} = 0.6577$ and $\mathrm{P} = 0.5783$. Recalling table 3 for degree of freedom, $df = 2$, it is considered that the difference is not statistically significant.

If the paired t-test is performed between mean length of fibers of pre and post RT datasets from table 5, I obtained $\mathrm{t} = 0.3225$ and $\mathrm{P} = 0.7776$. Again from table 3 for $df = 2$, it can be said that the difference of mean length of fibers between pre and post RT datasets is not statistically significant. But because of a lack of disease information, it is not

possible to make conclusions regarding the accuracy of the results and any improvement or degradation due to therapy. Simulation of a complete data set having information of pre-surgery, post surgery, and post radiation therapy should be studied in the future.

CHAPTER 5

CONCLUSION

Diffusion tensor imaging is a powerful tool for the visualization of white matter structures. The growing number of DTI-based studies and applications shows the great potential of this method. Although this method provides a better theoretical basis to address the complicated diffusion of water in white matter, the simulations are time-consuming and require considerable computational power. In this thesis, I have presented a comparison between deterministic and probabilistic tractography. I have shown the effectiveness of Gibbs tracking for global tractography which performs better in tracking crossing and kissing fibers. Compared with the other methods examined, the deterministic approach is computationally efficient, but probabilistic tractography can track longer fibers. I have also quantified various diffusion index values for a ROI near the corpus callosum, which can be used to assess different brain diseases.

The index values usually vary in the regions of brain, and for specific brain diseases. From the values of FA and ADC, we can differentiate between a normal and a diseased brain. Preoperative assessment of disease will help to detect the exact location of areas involved in surgery. In this study, multiple gradient direction data sets are taken which have positive effect on tracking though the time requirement for simulation increases with the gradient directions, which could limit the clinical application. For the accuracy of the measurements, we relied on expert knowledge obtained from St. Jude Children's Research Hospital. The simulation is done from different aspects such as changing the controlling parameters of the experiments such as fiber length, temperature, curvature angle, anisotropy value that gives different tractography results. So for getting a

reliable result, we need a gold standard tractography result which is a topic for future research.

In summary, I have investigated different tractography methods including deterministic, probabilistic, and global tractography and their pros and cons in this thesis. Simulation is done on DTI data sets having different gradient directions. In addition, I also quantified the radiation therapy effects on brain fibers based on the diffusion indices and mean length of fibers tracked.

REFERENCES

1. Derek K. Jones, “Diffusion MRI: Theory, Methods and Applications”, Oxford University Press, UK, Sep-2012, Ch. 5, pp. 69-72.
2. Basser PJ, Pierpaoli C, “A simplified method to measure the diffusion tensor from seven MR Images”, Magn Res Med 39:928–934, 1998.
3. Mark A. Horsfield and Derek K. Jones, “Application of diffusion-weighted and diffusion tensor MRI to white matter diseases-a review”, NMR biomed, 15(7-8):570-7, Nov-Dec. 2002
4. H. Nia, V. Kavcicb, T. Zhuc, S. Ekholma and J. Zhonga, C, “Effects of Number of Diffusion Gradient Directions on Derived Diffusion Tensor Imaging Indices in Human Brain”, AJNR 27: 1776-1781, Sept. 2006.
5. https://pursuit.unimelb.edu.au/features/deciphering-epilepsy/.
6. http://neuromedia.neurobio.ucla.edu/campbell/nervous/wp_images/182_TS_LP.gif)
7. Na Zhang, Zhen-Sheng Deng, Fang Wang and Xiao-Yi Wang, “The effect of different number of diffusion gradients on SNR of diffusion tensor-derived measurement maps”, J. Biomed. Sci and Engg, 96-101, Feb 2009.
8. Marco Reisert, Irina Mader, Valerij Kiselev et. al, “Global fiber reconstruction becomes practical”, NeuroImage 54, 955–962; (2011).
9. Mara Cercignani, Matilde Inglese et. Al., “Mean diffusivity and fractional anisotropy histograms of patients with multiple sclerosis”, AJNR 2001, 22:952-958.

10. M.S. Vishwas, B. C. Healy et al, “Diffusion tensor analysis of pediatric multiple sclerosis and clinically isolated syndromes,” AJNR 2013, 34:417-423

11. Mori S, Crain B, Chacko VP et. Al, “Three dimensional tracking of axonal projections in the brain” Ann Neurol 45:265–269, 1999.

12. S. Mori, and P.C.van Zijl. “Fiber tracking: principles and strategies–a technical review”. NMR Biomed, 15(7-8): 468-480, 2002.

13. *Technical and historical perspectives of remote sensing* by Nicholas M. short

14. *Diffusion imaging and fiber tractography* by Jennifer Campbell

15. J. Hennig and O. Speck (eds.), “High-Field MR Imaging: Medical Radiology, Diagnostic Imaging”, DOI: 10.1007/174_2011_161, © Springer-Verlag Berlin Heidelberg 2011.

16. M. A. Brown and R. C. Semelka, “MRI: Basic Principles and Applications”, Third Edition, ISBN 0-471-43310-1 © John Wiley & Sons, Inc. 2003.

17. D. M. Koh, H. C. Thoeny (Eds.), “Diffusion-Weighted MR Imaging: Applications in the body”, DOI: 10.1007/978-3-540-78576-7 © Springer-Verlag Berlin Heidelberg 2010.(book 7)

18. Chun-Hung Yeh et. al, “Diffusion microscopist simulator: A general Monte Carlo simulation system for diffusion magnetic resonance imaging”, PLoS ONE 8(10): e76626, doi: 10.1371/journal.pone.0076626, October 2013.

19. Parker, G. J.M., Haroon, H. A. and Wheeler-Kingshott, C. A.M., “A framework for a streamline-based probabilistic index of connectivity (PICo) using a structural interpretation of MRI diffusion measurements”, J. Magn. Reson. Imaging (2003), 18: 242–254. doi: 10.1002/jmri.10350.

20. T. E. J. Behrens, H. Johansen-Berg, S. Jbabdi, M. F. S. Rushworth, and M. W. Woolrich, “Probabilistic diffusion tractography with multiple fiber orientations. what can we gain?” NeuroImage, vol. 34, no. 1, pp. 144–155, 2007.

21. D. Tuch, “Q-ball imaging,” Magnetic Resonance in Medicine”, vol. 52, no. 6, pp. 1358–1372, 2004.

22. B. Jian and B. C. Vemuri, “A unified computational framework for deconvolution to reconstruct multiple fibers from diffusion weighted mri”, *IEEE Transactions on Medical Imaging*, vol. 26, no. 11, pp. 1464–1471, 2007.

23. Mori, S. and van Zijl, P.C.M., “Fiber tracking: Principles and strategies—A technical review”, NMR in Bio- medicine, **15**, 468-480, 2002..

24. Maxime Descoteaux et. al., “Deterministic and Probabilistic Tractography based on Complex Fiber Orientation Distributions”, Medical Imaging, *IEEE Transactions on* 28.2 (2009): 269-286.

25. Thomas E. Conturo et. al.,“Tracking neuronal fiber pathways in the living human brain”, Proc. Natl. Acad. Sci. USA Vol. 96, pp. 10422–10427, August 1999.

26. D.S. Tuch, V. J. Wedeen et. al., “A path integral approach to white matter tractography by”, Journal of mag. Res. Imaging 01/2000.

27. Le Bihan D., Mangin JF., Poupon C., and al. “Diffusion Tensor Imaging Concepts and Applications”, Journal of Magnetic Resonance Imaging, 2001.

28. Kreher BW., Mader I. et al.,” Gibbs tracking: a novel approach for the reconstruction of neuronal pathway,” Wiley Inter Science, 2008.

29. J. F. Mangin, P. Fillard, et. al., “Towards Global Tractography”, NeuroImage 80 (2013), 290-296.

30. Ola Friman et. al., " A Bayesian approach for stochastic white matter tractography", *IEEE Trans. on medical imaging,* vol. 25, no. 8, August 2006.

31. Mori S, Crain B, Chacko VP, van Zijl PCM, "Three dimensional tracking of axonal projections in the brain" Neurol 45:265–269, 1999.

32. Kirkpatrick, S.; Gelatt Jr, C. D.; Vecchi, M. P. (1983). "Optimization by Simulated Annealing". *Science* 220 (4598): 671–680.

33. Geoff J. M. Parker, Daniel Alexander, "Probabilistic Monte Carlo based mapping of cerebral connections utilizing whole brain crossing fiber information", Inform. Proc. in Medical Imaging 2003, LNCS 2732, pp. 684-695, 2003.

34. G. J. M. Parker, H. A. Haroon and C. Wheeler-Kingshott, "A framework for a streamline based probabilistic index of connectivity (PICo) using structural interpretation of MRI diffusion measurements", Journal of Mag. Res. Img, 18, 242-254, 2003.

35. P.A. Cook, D. C. Alexander, "Modeling uncertainty in two fiber orientation estimates within a voxel", Proc. Intl. Soc. Mag. Reson. Med. 14 (2006), pp. 1629.

36. Soares, J. M., Marques, P., Alves, V., and Sousa, N, "A hitchhiker's guide to diffusion tensor imaging", Front. Neurosci. 7:31. doi: 10.3389, 2013.

37. A.H. Poonawalla et. al., "Correction of Eddy currents in EPI-based diffusion tensor imaging", Proc. Intl. Soc. Mag. Reson. Med 9 (2001)

38. Mori S, Crain B, Chacko VP, van Zijl PCM, "Three dimensional tracking of axonal projections in the brain", Neurol 45:265–269, 1999.

39. Kreher BW., Mader I., and Kiselev VG. "Gibbs tracking: a novel approach for the reconstruction of neuronal pathway", Wiley Inter Science, 2008.

40. Jiang, Hangyi ei al., “DtiStudio: Resource program for diffusion tensor computation and fiber bundle tracking”, Computer methods and programs in Biomedicine, Vol. 81, Issue 2, 106-116 (2006).

41. P. B. Kingsley, “Introduction to diffusion tensor imaging mathematics: Part III. Tensor calculation, noise, simulations and optimization”, Concepts Magn. Reson, 28A: 155-179 (2006).

42. P. S. Yen, B. T. Teo et. al. “White matter tract involvement in brain tumors: A diffusion tensor imaging analysis”, surgical neurology 72, 2009.

43. P. B. Kingsley, “Introduction to diffusion tensor imaging mathematics: Part II. Anisotropy, Diffusion-weighting factors and gradient encoding schemes”, Concepts Magn. Reson, Part A, 28A: 123-154 (2006).

44. P.A. Cook, Y. Bai, et.al. “Camino: Open-source diffusion MRI reconstruction and processing”, 14th Scientific meeting of the Intl. Society for Magn. Reson. In medicine, Seattle, WA, USA, p. 2759, May 2006.

45. A. Henderson, ParaView Guide, “A Parallel Visualization Application”, Kitware Inc., 2007.

46. Sandor S and Leahy R, “Surface-based labeling of cortical anatomy using a deformable database”, *IEEE Transactions on Medical Imaging* 16(1):41-54. 1997.

47. Shattuck DW and Leahy RM, “BrainSuite: An Automated Cortical Surface Identification Tool”, Medical Image Analysis 8(2):129-142. 2002.

48. Paul A. Yushkevich, Joseph Piven, Heather Cody Hazlett, Rachel Gimpel Smith, Sean Ho, James C. Gee, and Guido Gerig, “User-guided 3D active contour

segmentation of anatomical structures: Significantly improved efficiency and reliability", Neuroimage. 2006 Jul 1; 31(3):1116-28. ITK SNAP

49. MRICRo: Rorden, C., Brett, M., "Stereotaxic display of brain lesions", Behavioural neurology. 12, 191-200, (2000).

50. Kreher, B., Henning, J. and Il'yasov, K. (2006) "DTI&Fiber-Tools: A complete toolbox for DTI calculation, fiber tracking, and combined evaluation", Proceeding of ISMRM 14th International Scientific Meeting, Seattle.

51. S. Mohammadi, H. E. Möller, H. Kugel, D. K. Müller, and M. Deppe, "Correcting eddy current and motion effects by affine whole-brain registrations: evaluation of three-dimensional distortions and comparison with slicewise correction," Magnetic Resonance in Medicine, vol. 64, no. 4, pp. 1047-1056, Oct. 2010.

52. Karl J. Friston, John T. Ashburner, Stephen Kiebel, Thomas E. Nichols, William D. Penny, "Statistical Parametric Mapping: The Analysis of Functional Brain Images", *Elsevier/Academic Press: Amsterdam, 2007

53. W.H. Beyer, "CRC Standard Mathematical Tables", 28th ed., Boca Raton, FL: CRC Press , pp 536 and 571, 1987.

Appendix

Table A: Gradient directions or orientation information for 12 D 4 averages data set

x	Y	z
0.000000000000000	0.000000000000000	0.000000000000000
0.862981081008911	-0.365167051553726	0.349165558815002
0.862981081008911	0.365167051553726	0.349165558815002
0.862981081008911	0.365167051553726	-0.349165558815002
0.862981081008911	-0.365167051553726	-0.349165558815002
0.358699887990952	-0.365254640579224	-0.859024584293365
0.356550574302673	-0.867405891418457	-0.347100108861923
0.356612652540207	-0.866849601268768	0.348423719406128
0.358914166688919	-0.365450441837311	0.858851909637451
0.358914166688919	0.365450441837311	0.858851909637451
0.356612652540207	0.866849601268768	0.348423719406128
0.356550574302673	0.867405891418457	-0.347100108861923
0.358699887990952	0.365254640579224	-0.859024584293365
0.000000000000000	0.000000000000000	0.000000000000000
0.862981081008911	-0.365167051553726	0.349165558815002
0.862981081008911	0.365167051553726	0.349165558815002
0.862981081008911	0.365167051553726	-0.349165558815002
0.862981081008911	-0.365167051553726	-0.349165558815002
0.358699887990952	-0.365254640579224	-0.859024584293365
0.356550574302673	-0.867405891418457	-0.347100108861923
0.356612652540207	-0.866849601268768	0.348423719406128
0.358914166688919	-0.365450441837311	0.858851909637451
0.358914166688919	0.365450441837311	0.858851909637451
0.356612652540207	0.866849601268768	0.348423719406128
0.356550574302673	0.867405891418457	-0.347100108861923
0.358699887990952	0.365254640579224	-0.859024584293365
0.000000000000000	0.000000000000000	0.000000000000000
0.862981081008911	-0.365167051553726	0.349165558815002
0.862981081008911	0.365167051553726	0.349165558815002
0.862981081008911	0.365167051553726	-0.349165558815002
0.862981081008911	-0.365167051553726	-0.349165558815002
0.358699887990952	-0.365254640579224	-0.859024584293365
0.356550574302673	-0.867405891418457	-0.347100108861923
0.356612652540207	-0.866849601268768	0.348423719406128
0.358914166688919	-0.365450441837311	0.858851909637451
0.358914166688919	0.365450441837311	0.858851909637451
0.356612652540207	0.866849601268768	0.348423719406128
0.356550574302673	0.867405891418457	-0.347100108861923
0.358699887990952	0.365254640579224	-0.859024584293365
0.000000000000000	0.000000000000000	0.000000000000000
0.862981081008911	-0.365167051553726	0.349165558815002
0.862981081008911	0.365167051553726	0.349165558815002
0.862981081008911	0.365167051553726	-0.349165558815002
0.862981081008911	-0.365167051553726	-0.349165558815002
0.358699887990952	-0.365254640579224	-0.859024584293365
0.356550574302673	-0.867405891418457	-0.347100108861923
0.356612652540207	-0.866849601268768	0.348423719406128
0.358914166688919	-0.365450441837311	0.858851909637451
0.358914166688919	0.365450441837311	0.858851909637451
0.356612652540207	0.866849601268768	0.348423719406128
0.356550574302673	0.867405891418457	-0.347100108861923
0.358699887990952	0.365254640579224	-0.859024584293365